2018

The Employment of Electrolyte Additives to Overcome the Limitations of Li-ION Batteries

Mickdy S. Milien
University of Rhode Island, mickdy28@gmail.com

THE EMPLOYMENT OF ELECTROLYTE ADDITIVES TO OVERCOME THE LIMITATIONS OF LI-ION BATTERIES

BY

MICKDY S. MILIEN

A DISSERTATION SUBMITTED IN PARTIAL FULFILLMENT OF THE REQUIREMENTS FOR THE DEGREE OF

DOCTOR OF PHILOSOPHY

IN

CHEMISTRY

UNIVERSITY OF RHODE ISLAND

2018

DOCTOR OF PHILOSOPHY DISSERTATION

OF

MICKDY S. MILIEN

APPROVED:

Dissertation Committee:

Major Professor Brett L. Lucht

William B. Euler

David R. Heskett

Nasser H. Zawia
DEAN OF THE GRADUATE SCHOOL

UNIVERSITY OF RHODE ISLAND
2018

ABSTRACT

Due to the shift towards sustainable energy, lithium ion batteries (LIB) have amassed significant interest from the automobile industry. In order to power the large format batteries required for electric vehicles (EV), higher energy density materials are being developed, however challenges such as interfacial resistance of the anode materials and undesirable reactions of the electrolyte with the surface of both electrode materials threatens the power, safety, and lifetime of batteries containing these materials. While there are numerous research efforts dedicated to improving the materials themselves, this work focuses on the *in-situ* surface modification of the electrode materials by incorporating electrolyte additives, which get sacrificially reduced or oxidized to form stable surface films. The novel organophosphorous additive, lithium dimethyl phosphate (LiDMP), has been investigated as an anode-film forming additive, which decreases impedance in $LiNi_{1/3}Mn_{1/3}Co_{1/3}O_2$/graphite cells, the fluorinated organophosphorous additive, lithium bis(2,2,2-tifluoroethyl)phosphate (LiBFEP), has been investigated as a cathode-film forming additive; which hinders manganese dissolution from the cathode and prevents continuous oxidation of the electrolyte in $LiNi_{0.5}Mn_{1.5}O_4$/graphite cells; and imides and borates have been investigated as anode-film forming additives, which prevent the catalytic reduction of the electrolyte, thus hindering gassing in $Li_4Ti_5O_{12}/LiMn_2O_4$ cells. Electrochemical impedance spectroscopy, X-ray photoelectron spectroscopy, and ATR-IR spectroscopy have been used to gain an understanding of the surface films formed with and without the additives while *in-situ* gas measurements based on Archimedes'

principle and gas chromatography have given insight into how the implementation of the imides and borates affect gassing. The knowledge obtained from this work enables selective design of LIB with various chemistries to enable performance while maintaining full function of materials.

ACKNOWLEDGMENTS

This thesis is dedicated to my mother, Simone Milien. You were my first teacher and you've never failed to encourage me (or any of your children) to explore, learn, and grow. Friends, colleagues, and people that have gotten to know me throughout my life have always expressed both respect and appreciation for you although they've never met you (I remember thinking as a child: "you don't even know her!"). I've recently learned that all 4 of my brothers have had similar experiences.

You are inspired and an inspiration, a phenomenal woman, mother, and human being.

Thank You.

I'd like to thank my advisor, Professor Brett Lucht for his guidance throughout the past 4 years. Many thanks to past and present post docs for encouraging me to ask all of my questions and for the countless fruitful discussions which allowed me to arrive at most of the answers. I'd like to thank my committee members for their time and patience.

Lastly, I'd like to thank my family, friends, and various teachers who have never failed to nourish my curiosity.

PREFACE

This thesis was written in manuscript format. Chapter 1 is an introduction to lithium ion batteries, Chapter 2 was published in the Journal of the Electrochemical Society, and manuscripts for Chapters 3 and 4 are in progress and will be published shortly.

TABLE OF CONTENTS

CHAPTER 1

INTRODUCTION

Background

Lithium's high theoretical capacity (3,829 mAh/g) as well as the poor coulombic efficiency (ratio the battery stored to the ratio of charge the battery delivered) and safety issues associated with lithium anode-containing rechargeable batteries has indirectly lead to the success of lithium ion batteries (LIB). [1] While the research dedicated to developing intercalation compounds as cathode materials (from TiS_2 to $LiCoO_2$) was the preparation, the demand for an anode material to replace lithium metal, opportunity, lead to graphite (also an intercalation compound; LiC_6). [1-2] Due to the electrochemical instability (at lower potentials) of the aprotic organic solvents used, continuous reduction of the electrolyte on graphite's surface was a problem until the solvent ethylene carbonate (EC) was added to electrolyte formulations. The reduction products of EC form an electrically insulating but ionically conductive solid electrolyte interface (SEI), which passivates the surface of graphite in the initial cycles and prevents further electrolyte reduction. [1-4] Since their employment as the power source for consumer electronics by SONY in 1991, LIB have dominated as the power source for consumer electronics, and has drawn great interest from the automotive industry. As far as LIB for electric vehicles, the goal is to increase the power and energy density of the battery, making it possible to decrease the pack size, and thus decreasing the price per customer. [5] Currently a compromise has to be reached

between power and energy density, and this is a function of the design of the battery and the materials used. [1]

Working Principle of LIB

The main components of a LIB are the cathode, anode, and electrolyte. The cathode hosts Li ions within its matrix and is separated from the anode with a separator to prevent short circuits. When charging a battery, voltage is applied and the lithium ions are shuttled from the cathode (where oxidation occurs) through the electrolyte (accompanied by electrons which travel through the external circuit) and inserted into the anode (where reduction occurs). [6] This process occurs reversibly as the battery is discharged (spontaneously); the lithium ions are shuttled from the anode, through the electrolyte, and back into the cathode. Representative chemical equations are as follows:

Cathode ($LiCoO_2$): $LiCoO_2 \leftrightarrow Li_{1-x}CoO_2 + Li^+ + x\ e^-$

Anode (Graphite): $C_6 + x\ Li^+ + x\ e^- \leftrightarrow x\ LiC_6$

Net Equation: $LiCoO_2 + C_6 \leftrightarrow Li_{1-x}CoO_2 + x\ LiC_6$

Cathode

The positive electrodes (accepts electrons during discharge) in LIB are materials with higher working potentials (*vs*. Li/Li^+), which host the lithium ions that get shuttled back and forth between the cathode and the anode. Cathode materials are lithiated transition metal oxides with the formula LMO where L = lithium, M =

manganese (Mn), nickel (Ni), and/or cobalt (Co), and O = oxygen, which are prepared in the lithiated state. $LiCoO_2$ (LCO) cathodes, which have a specific capacity of 140 mAh/g and working potential of 3.9 V (*vs*. Li/Li^+) were the cathodes originally used in commercialized LIB, however due to LCO's structural instability upon extracting too much ($x < \sim 0.5$) lithium as well as the cost and toxicity of Co, $Li[Ni_{1/3}Co_{1/3}Mn_{1/3}]O_2$ (NMC111) (working potential of 3.8 V (*vs*. Li/Li^+) and theoretical capacity of 160 mAh/g) become a conventional cathode material. [1] The need for higher energy density has lead to the development of high energy density cathode materials such as nickel-rich layered oxides ($LiNi_xMn_yCo_zO_2$), lithium-rich layered oxides ($0.6Li_2MnO_3$-$0.4Li(Ni_{1/}3Co1/3Mn_{1/3})O_2$), and high voltage spinel ($LiNi_{0.5}Mn_{1.5}O_4$) (LNMO), however structural instability of the materials themselves as well as the electrochemical instability of the electrolyte at the potentials required to obtain high energy from these materials are the focus of current research. [1, 7-12]

Anode

The negative electrodes in LIB are materials with low working potentials, which are capable of accommodating Li ions via insertion (for layered materials such as graphite) or intercalation (for spinel structures such as $Li_4Ti_5O_{12}$ (LTO). Due to its low working potential (~0.2 V *vs*. Li/Li^+), low cost, and good cycle life (once the SEI is formed) graphite is currently the most widely used anode material. [2, 13-14] Capacity fading at high C rates is attributed to the slow kinetics involved with lithium intercalation into graphite. [15] Due to the lagging kinetics involved in intercalation, the higher the rate, the less lithium is inserted into the graphite, resulting in diminished

capacity as the rate increases. [16] While graphite material contains conductive carbon to improve its conductivity, when a passivation film is formed on the surface of graphite, the conductivity of this passivation layer affects charge-transfer as well. [17] Cells containing LTO, an anode material of interest for power applications, operates at a potential higher than the reduction potential of the electrolyte and doesn't require a passivation film, however this limits the voltage window when paired with conventional cathodes such as LCO and NMC111. LTO also suffers from gassing at elevated temperatures. [18]

Electrolyte

The electrolyte consists of lithium hexafluorophosphate ($LiPF_6$) salt dissolved in a mixture of linear (ethyl methyl carbonate (EMC), dimethyl carbonate (DMC), or diethyl carbonate (DEC)) and cyclic carbonates (EC). While $LiPF_6$ is both chemically and thermally unstable, it's currently the only salt that meets all of the necessary requirements (fully dissociates in solution, passivates the aluminum current collector, and possesses a wide electrochemical stability window) of the electrolyte salt. [3] Due to its high dielectric constant and ability to form the SEI, EC is a widely used electrolyte solvent. [3] EC is extremely viscous, thus the low viscosity linear carbonates are mixed with EC to lower the viscosity of the solvent. The electrochemical stability window (ESW) of the electrolyte is of paramount importance to the performance of LIB. Graphite's working potential is outside of the ESW of the electrolyte solvents, thus the electrolyte would be continuously reduced if not for the formation of the SEI during early cycles. The higher potentials used with high energy

cathode materials is also outside the ESW of the electrolyte solvents, thus the formation of a cathode electrolyte interface (CEI) is necessary in order to prevent continuous oxidation of the electrolyte on the surface of the cathode.

Review of the problem

The main challenges associated with powering electric vehicles are power, safety, operation in various temperature ranges, and lifetime. [5] All of which are dependent on both the individual and synergistic function of the anode, cathode, and electrolyte. This thesis presents the investigation of electrolyte additives as surface modification tools harnessed to overcome challenges of the components of the battery such as interfacial resistance of the electrode materials, electrochemical instability of the electrolyte, and unwanted reactions of the electrolyte with the surface of the electrode materials.

References

1. Meyers, R. A., *Encyclopedia of Sustainability Science and Technology*. 2012.
2. Goodenough, J. B., Rechargeable batteries: challenges old and new. *Journal of Solid State Electrochemistry* **2012,** *16* (6), 2019-2029.
3. Xu, K., Electrolytes and Interphases in Li-Ion Batteries and Beyond. *Chemical Reviews* **2014,** 114 (23), 11503-11618.
4. Fong, R.; von Sacken, U.; Dahn, J.R.; Studies of lithium intercalation into carbons using nonaqueous electrochemical cells. *Journal of the Electrochemical Society* **1990,** 137, 2009-2013.
5. Lamp, P., "Advanced Materials for Future Generations of Automotive Batteries: Potentials and Limits." PowerPoint Presentation. IMLB, June 2016.
6. Scrosati, B., Abraham, K.M., Van Schalkwijk, W., Hassoun, J. *Lithium Batteries: Advanced Technologies and Applications.* 2013.
7. Xu, B.; Qian, D.; Wang, Z.; Meng, Y. S., Recent progress in cathode materials research for advanced lithium ion batteries. *Materials Science and Engineering: R: Reports* **2012,** *73* (5-6), 51-65.
8. Jung, R.; Metzger, M.; Maglia, F.; Stinner, C.; Gasteiger, H. A., Oxygen Release and Its Effect on the Cycling Stability of LiNixMnyCozO2(NMC) Cathode Materials for Li-Ion Batteries. *Journal of The Electrochemical Society* **2017,** *164* (7), A1361-A1377.
9. Son, M. Y.; Lee, J. K.; Kang, Y. C., Fabrication and electrochemical performance of 0.6Li2MnO3-0.4Li(Ni1/3Co1/3Mn1/3)O2 microspheres by two-step spray-drying process. *Sci Rep* **2014,** *4*, 5752.

10. Kozawa, T.; Murakami, T.; Naito, M., Insertion of lattice strains into ordered LiNi0.5Mn1.5O4 spinel by mechanical stress: A comparison of perfect versus imperfect structures as a cathode for Li-ion batteries. *Journal of Power Sources* **2016,** *320*, 120-126.

11. Gallagher, K. G.; Croy, J. R.; Balasubramanian, M.; Bettge, M.; Abraham, D. P.; Burrell, A. K.; Thackeray, M. M., Correlating hysteresis and voltage fade in lithium- and manganese-rich layered transition-metal oxide electrodes. *Electrochemistry Communications* **2013,** *33*, 96-98.

12. Choi, N.-S.; Han, J.-G.; Ha, S.-Y.; Park, I.; Back, C.-K., Recent advances in the electrolytes for interfacial stability of high-voltage cathodes in lithium-ion batteries. *RSC Adv.* **2015,** *5* (4), 2732-2748.

13. Scrosati, B.; Garche, J.; Lithium batteries: status, prospects, and future. *Journal of Power Sources* **2010,** 195 (9), 2419-2430.

14. Marom, R.; Amalraj, S.F.; Leifer, N.; Jacob, D.; Aurbach, D.; A review of advanced and practical lithium battery materials *Journal of Materials Chemistry* **2011,** 21, 9938-9954.

15. Tran, T.D.; Feikert, J.H.; Pekala, R.W.; Kinoshita, K.; Rate effect on lithium-ion graphite electrode performance. *Journal of Applied Electrochemistry* **1996,** (11), 1161-1167.

16. Ahn, S.; Kim, Y.; Kim, K.J.; Kim, T.H.; Lee, H.; Kim, M.H.; Development of High Capacity, High Rate Li+ ion Batteries Utilizing Metal Fiber Conductive Additives *Journal of Power Sources* **1999,** 82, 896-901.

17. Zaghib, K.; Brocgu, F.; Guerfi, A.; Kinoshita, K.; Effects of particle size on lithium intercalation rates in natural graphite *Journal of Power Sources* **2001,** 103, 140-146.

18. He, M.; Castel, E. ; Laumann, A.; Nuspl, G.; Novak, P. ; Berg, E. J. ; In Situ Gas Analysis of Li4Ti5O12 Based Electrodes at Elevated Temperatures *Journal of The Electrochemical Society* **2015,** 162 (6), A870-A876.

CHAPTER 2

DEVELOPMENT OF LITHIUM DIMETHYL PHOSPHATE AS AN ELECTROLYTE ADDITIVE FOR LITHIUM ION BATTERIES

by

Mickdy S. Milien[1]; Usha Tottempudi[2]; Miyoung Son[3]; Makoto Ue[3]; Brett L. Lucht[4]

is published in The Journal of The Electrochemical Society

---

[1] PhD Candidate, Department of Chemistry, The University of Rhode Island, Kingston, RI 02882. Email: mmilien@chm.uri.edu

[2] Post Doctoral Associate, Department of Chemistry, The University of Rhode Island, Kingston, RI 02881

[3] Battery R&D Center, Samsung SDI, 130 Samsung-ro, Yeongtong-gu, Suwon-si, Gyeonggi-do, 443-803, South Korea

[4] Professor, Department of Chemistry, The University of Rhode Island, Kingston, RI 02881. Email: blucht@chm.uri.edu

Abstract

The novel electrolyte additive lithium dimethyl phosphate (LiDMP) has been synthesized and characterized. Incorporation of LiDMP (0.1 % wt.) into $LiPF_6$ in ethylene carbonate (EC) / ethyl methyl carbonate (EMC) (3:7 wt.) results in improved rate performance and reduced impedance for graphite / $LiNi_{1/3}Mn_{1/3}Co_{1/3}O_2$ cells. Ex-situ surface analysis of the electrodes suggests that incorporation of LiDMP results in a modification of the solid electrolyte interphase (SEI) on the anode. A decrease in the concentration of lithium alkyl carbonates and an increase in the concentration of lithium fluoro phosphates are observed. The change in the anode SEI structure is responsible for the increased rate performance and decreased cell impedance.

Introduction

Lithium ion batteries (LIB) are currently the preferred source of power for consumer electronics such as mobile phones, computers, and cameras and are of interest for large-scale high-powered battery markets including aerospace, military, and electric vehicles. The reaction of non-aqueous electrolytes on the surface of the anode during the first few charging cycles results in the generation of a solid electrolyte interphase (SEI), which is critical to the performance of LIB. [1] While the structure and function of the anode SEI is still poorly understood, lithium ion intercalation through the SEI and into the anode is one of the largest limitations for high rate performance. [2-5]

Electrolyte additives have been used to modify the structure of the SEI and improve the performance of LIB via decreasing the irreversible capacity during formation, lowering SEI resistance, or stabilizing cells against extreme conditions such as high temperature and high rate cycling. [1, 6-8] Vinylene carbonate (VC) is one of the most frequently investigated additives and has been used to generate a more stable SEI on graphite, but unfortunately the films are typically more resistive. [9] Improving the kinetics of lithium ion batteries has been investigated via incorporation of alternative co-solvents to improve electrolyte conductivity [10]or incorporation of electrolyte additives, such as propane sultone (PS), to reduce the impedance of the SEI. [11] Recently, novel phosphorus additives have been reported to improve the interfacial kinetics of the anode SEI. [12] In this manuscript, we report on the development of a novel organophosphorous additive, lithium dimethyl phosphate

(LiDMP), which has been found to function as an anode film-forming additive, which decreases cell impedance.

Experimental

Materials

All of the materials for the synthesis of LiDMP were purchased from Sigma Aldrich or Acros and used without further purification. Battery-grade ethylene carbonate (EC), ethyl methyl carbonate (EMC), and lithium hexafluorophosphate ($LiPF_6$) were provided by BASF, Germany, and used as received. LiDMP was washed and filtered 3 times and its purity was assessed from ^{1}H and ^{31}P NMR spectroscopy.

Synthesis of LiDMP

Trimethyl phosphate 1.75 mL (14.9 mmol) was added, drop wise, to a solution of lithium iodide 2.00 g (14.9 mmol) in 100 mL of acetone and allowed to stir for 2 days in a nitrogen-filled glove box resulting in the generation of a precipatate. [13] The contents of the flask were filtered through a glass filter frit funnel to collect the precipitate. The precipitate was transferred to a round bottom flask, 15 mL of acetone was added, and the solution was allowed to stir for 2 hours to wash the crude product. The method above was repeated twice and the salt was dried over night under nitrogen on the schlenk line to yield LiDMP (1.76 g, white solid, 89 % yield). ^{1}H NMR (300 MHz, D_2O): δ 3.54 (d, 6H, J = 27 Hz). ^{31}P NMR (300 MHz, D_2O): δ 2.98 (sept, J = 27 Hz).

Coin Cell Preparation

Lithium ion coin cells containing an artificial graphite anode and a $LiNi_{1/3}Mn_{1/3}Co_{1/3}O_2$ cathode were prepared with 1.2 M $LiPF_6$ in EC: EMC (3:7 by volume, standard electrolyte, STD) with and without 0.1% (wt.) added LiDMP. The negative electrodes were composed of 95.7% (wt.) graphite, 3.8% (wt.) carboxymethyl cellulose (CMC-SBR) binder, and 0.5% (wt.) conductive carbon (Super P). The positive electrodes were composed of 93% (wt.) $LiNi_{1/3}Mn_{1/3}Co_{1/3}O_2$, 4% (wt.) polyvinylidene fluoride (PVDF) binder, and 3% (wt.) conductive carbon. The coin cells were prepared with 105 μL electrolyte, 2 separators (a polyethylene film and a glass fiber).

Electrochemical Testing

Coin cells were cycled with a constant current-constant voltage charge and a constant current discharge between 4.2 V and 3.0 V using a battery cycler (BT-2000 Arbin cycler, College Station, TX). The cells were cycled with the following formation procedure: first cycle at C/20, D/20, second and third cycles at C/10, D/10, and the fourth and fifth cycles at C/5, D/5. After the initial five formation cycles the cells were cycled at a C/5, D/5 rate for 15 cycles at room temperature, followed by 3 cycles each of C/3, D/3, C/2, D/2, C, D, 2C, 2D, 3C, 3D, 5C, 5D, and C/5, D/5, respectively.

All cells were prepared in duplicate to confirm reproducibility of the cycling behavior. Representative cycling data are presented. After 20 cycles, electrochemical impedance spectroscopy (EIS) was measured at a 0% state of charge on a Solartron SI

1287 electrochemical interface and SI 1252A frequency response analyzer with an AC perturbation of 10 mV and frequency range of 300 kHz - 30 mHz. Cells were then cycled at elevated rates, allowed to rest in order to obtain equilibrium, and EIS measurements were repeated.

In order to measure the impedance of symmetrical graphite and symmetrical NCM 111 cells, 4 cells containing the standard electrolyte were assembled using the method previously mentioned. The cells were charged to 4.2V, allowed to rest, and opened. The electrodes were harvested and 2 symmetrical lithiated graphite cells as well as 2 symmetrical delithiated NCM111 cells were assembled in the method previously mentioned, allowed to rest in order to obtain equilibrium, and analyzed in-situ via EIS using the parameters previously mentioned. Symmetric cells were prepared from electrodes cycled with standard electrolyte with and without added LiDMP.

Ex-situ Surface Analysis

The cells were disassembled in an argon glove box. The electrodes were rinsed with dimethyl carbonate (DMC) three times to remove residual EC and $LiPF_6$ and evacuated overnight prior to surface analysis. X-ray photoelectron spectroscopy (XPS) was acquired with a Thermo K-alpha system using Al Kα radiation ($h\upsilon$ = 1486.6 eV) under ultra high vacuum and a measured spot size of 400 μm. Samples were transferred into the XPS chamber with a vacuum transfer vessel. The binding energy was corrected based on the C 1s of C-C at 284.3 eV. The spectra obtained were analyzed using Thermo Advantage software (version 5.926). A mixture of 30%

Laurentzian and 70% Gaussian functions was used for the least-squares curves fitting procedure.

Results and Discussion

Electrochemical Testing

A comparative study of $LiNi_{1/3}Mn_{1/3}Co_{1/3}O_2$/Graphite cells with the standard electrolyte and the standard electrolyte with 0.1% (wt.) of added LiDMP was conducted in order to assay the effect of the additive on cycling behavior. Capacity retention and rate performance of cells cycled with and without LiDMP are displayed in Figure 2.2. Although both sets of cells display similar capacity retention at low rates, cells cycled with LiDMP exhibit a higher first coulombic efficiency (CE) of 91.5% compared to 87.9% of cells cycled with the standard electrolyte. The improved rate performance of the standard electrolyte with added LiDMP at 2C and 3C suggests that there is less resistance, with LiDMP

The voltage profile of the NCM111/Graphite cells at C/3 and 2C are displayed in Figure 2.3. The cell with added LiDMP has comparable capacity to the cell with the standard electrolyte at C/3 and significantly more capacity at 2C. The larger voltage hysteresis observed for the cell cycled with standard electrolyte provides further support for reduced cell resistance with added LiDMP. The passivation film generated for the cell cycled with LiDMP is more conductive than that generated without LiDMP. This is demonstrated by the decrease in ohmic potential drop observed in the 2C discharge curve in Figure 2 of the cell cycled with 0.1% (wt.) LiDMP.

Impedance measurements of the NCM111/Graphite cells, which have undergone formation at 25^{o}C, with and without LiDMP, are displayed in Figure 2.4a. The cells cycled with added LiDMP have lower impedance than the cells cycled with the standard electrolyte, consistent with the rate data. Again, this is attributed to the LiDMP-derived surface film, which improves charge-transfer. In order to determine whether the improved resistance is due to changes with the anode or the cathode, symmetrical cells of lithiated graphite and delithiated NCM111 were constructed. The impedance measurements of the symmetrical cells are displayed in Figures 2.4b and 2.4c, respectively. The graphite symmetrical cell with added LiDMP has significantly less resistance than the graphite symmetrical cell with the standard electrolyte (Figure 2.4b) while the NCM111 symmetrical cells have similar impedance with and without added LiDMP (Figure 2.4c), this demonstrates that the reduced resistance is a function of the LiDMP modifying the SEI on the anode.

Surface Characterization

The relative atomic concentrations of elements detected on the surface of fresh graphite electrodes and graphite electrodes extracted from cells which have undergone formation cycling at 25^{o}C with the standard electrolyte (STD) and STD with added LiDMP are shown in Figure 2.5. The electrode cycled with the standard electrolyte has an increase in the concentration of O, F and P, and a decrease in the concentration of C, supporting the generation of an SEI on the surface of the active material. Similar results are observed for the cell cycled with the electrolyte with added LiDMP except there is a greater increase in the concentrations of O, F, and P, and a greater decrease

in the concentration of C, which suggests a structural modification of the SEI upon incorporation of LiDMP.

The C1s XPS spectra of fresh graphite electrode and the graphite electrodes cycled with the standard electrolyte with and without added LiDMP are displayed in Figure 2.6. A decrease in the intensity of the C-C peak (284.3 eV) combined with the increases in the intensity of the C-H (285.6 eV), C-O (286.0 eV), CO_2 (288.1 eV), and CO_3 (290.1 eV) peaks indicates that an organic passivation layer generated from the reduction of EC covers the graphite electrode. [3] Related peaks associated with C-H, C-O, and CO_3 are observed on the surface of the electrode cycled with added LiDMP, but the intensity of the new absorptions are weaker, consistent with less EC reduction on the anode surface.

The F1s XPS spectra are very similar for both the electrode cycled with the standard electrolyte and the electrode cycled with added LiDMP. Small amounts of $Li_xPO_yF_z$ (687.2 eV) and larger amounts of LiF (685.0 eV) are present on the surface of both electrodes. The O1s XPS spectra differ in that the electrode cycled with LiDMP displays small amounts of Li_2O (528.8 eV), significantly less C-O species (533.0 eV), and a significantly greater peak at 531.6 eV, which corresponds to the binding energy of Li_3PO_4. [14]

The P2p XPS spectra of the electrode cycled with the standard electrolyte with and without added LiDMP are provided in Figure 2.6. The electrode cycled with the standard electrolyte has a low concentration of residual $LiPF_6$ and/or $Li_xPO_yF_z$ at 138.0 eV and low concentration of phosphates at 134.0 eV. The electrode cycled with electrolyte containing added LiDMP also has a low concentration of $LiPF_6$ and/or

$Li_xPO_yF_z$, but the concentration of phosphates are significantly greater, consistent with deposition of LiDMP reduction products on the surface of the anode. The increased concentration of phosphates likely correlates with the reduced impedance of the cycled anodes. Similar observations have been observed with other additives that generate phosphate or sulfate rich SEIs. [12,15]

Conclusion

The novel lithium salt, lithium dimethyl phosphate (LiDMP), was synthesized and investigated as an anode film forming electrolyte additive. Incorporation of LiDMP into a standard electrolyte formulation results in improved first cycle efficiency, improved rate performance and decreased cell impedance on the graphitic anode. Ex-situ surface analysis of the cycled anodes reveals lower concentrations of lithium alkyl carbonates, consistent with the improved efficiency, and a higher concentration of $Li_xPO_yF_z$ on electrodes cycled with added LiDMP. The presence of higher concentrations of $Li_xPO_yF_z$ in the anode SEI is likely the source of improved first cycle efficiency and reduced impedance. Similar improvements have been reported for additives, which result in the generation of phosphate or sulfate rich SEIs.

Acknowledgements

We thank Samsung SDI for financial support of this work. We also acknowledge funding from Department of Energy Office of Basic Energy Sciences EPSCoR Implementation award (DE-SC0007074) for the XPS.

References

1. K. Xu, *Chem. Rev*., **114,** 11503 (2014).
2. P. Verma, P. Maire, P. Novak, *Electrochim. Acta.,* **55,** 6332 (2010).
3. M. Nie, D. Chalasani, D. P. Abraham, Y. Chen, A. Bose, B. L. Lucht, *J. Phys. Chem. C,* **117,** 1257 (2013).
4. F. Puglia, R. Gitzendanner, C. Marsh, T. Curran, *J. Power Sources,* **96,** 40 (2001).
5. Y. Yamada, Y. Iriyama, T. Abe, Z. Ogumi, *Langmuir,* **25,** 12766 (2009).
6. K. Zaghib, M. Dontigny, A. Guerfi, P. Charest, I. Rodrigues, A. Mauger, C.M. Julien, *J. Power Sources,* **196,** 3949 (2011).
7. H. W. Rollins, M.K. Harrup, E. J. Dufek, et al. *J. Power Sources,* **263,** 66 (2014).
8. S. Menkin, D. Golodnitsky, E. Peled, *Electrochem. Commun*., **11,** 1789 (2009).
9. Y. Qin, Z. Chen, J. Liu, K. Amine, *Electrochemical and Solid-State Letters,* **13,** A11 (2010).
10. M. C. Smart, B. V. Ratnakumar, K. B. Chin, L. D. Whitcanack, *J. Electrochem. Soc.*, **157(12),** A1361 (2010).
11. M. Q. Xu, W. S. Li, B. L. Lucht, *J. Power Sources*, **193,** 804 (2009).
12. K.-E. Kim, J. Y. Jang, I. Park, M.-H. Woo, M.-H. Jeong, W. C. Shin, M. Ue, N.-S. Choi *Electrochm. Comm*., **61,** 121 (2015).
13. M. Mentz, A.M. Modro, T.A Modro, *J. Chem. Research* (S), **1,** 46 (1994).

14. A.C. Kozen, A.J. Pearse, C. Fu, M. Noked, G.W. Rubloff, *Chem. Mater*., **27,** 5324 (2015).

15. B. Zhang, M. Metzger, S. Solchenbach, M. Payne, S. Meini, H. Gasteiger, A. Garsuch, B. L. Lucht, *J. Phys. Chem. C.,* **119,** 11337 (2015).

Figures

Figure 2.1

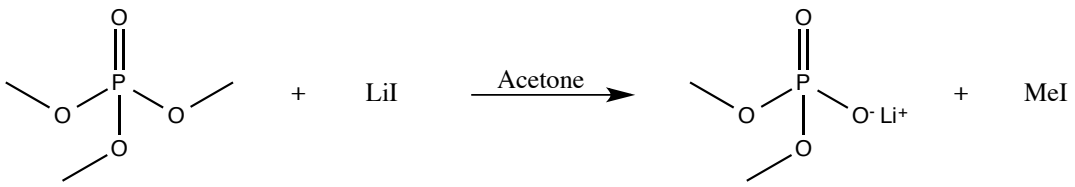

Figure 2.1: Synthesis of LiDMP.

Figure 2.2

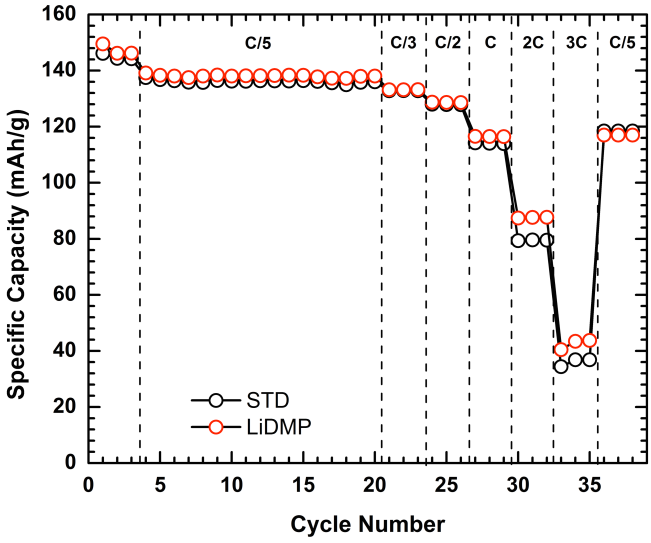

Figure 2.2: Cycling retention and rate performance of $LiNi_{1/3}Co_{1/3}Mn_{1/3}O_2$/Graphite cells at 25°C with the baseline electrolyte (STD) and with the baseline + LiDMP.

Figure 2.3

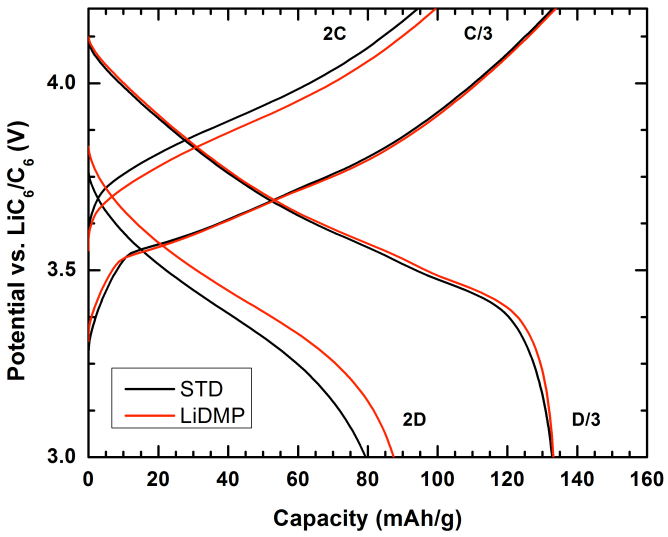

Figure 2.3: Voltage profile of $LiNi_{1/3}Co_{1/3}Mn_{1/3}O_2$/Graphite cells at 25°C (C/3, D/3, 2C, and 2D between 3.0V and 4.2V) with the baseline electrolyte (STD) and the baseline + LiDMP.

Figure 2.4

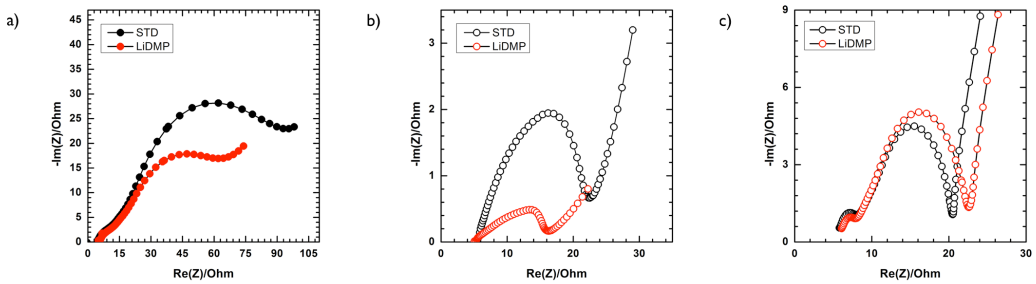

Figure 2.4: EIS measurements at OCV of a) $LiNi_{1/3}Co_{1/3}Mn_{1/3}O_2$/Graphite cells which have undergone formation cycling at 25°C (0% SOC), b) Symmetrical lithiated graphite cells, and c) Symmetrical delithiated NCM111.

Figure 2.5

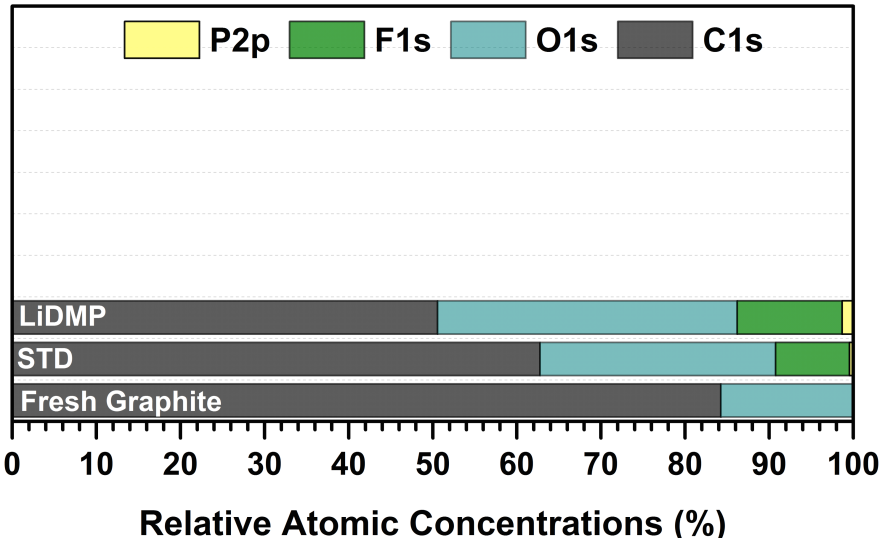

Figure 2.5: Relative atomic concentrations of elements detected on the surface of the fresh anode, the anode which has undergone formation cycling at 25°C with the baseline electrolyte, and the anode which has undergone formation cycling with the baseline electrolyte + LiDMP.

Figure 2.6

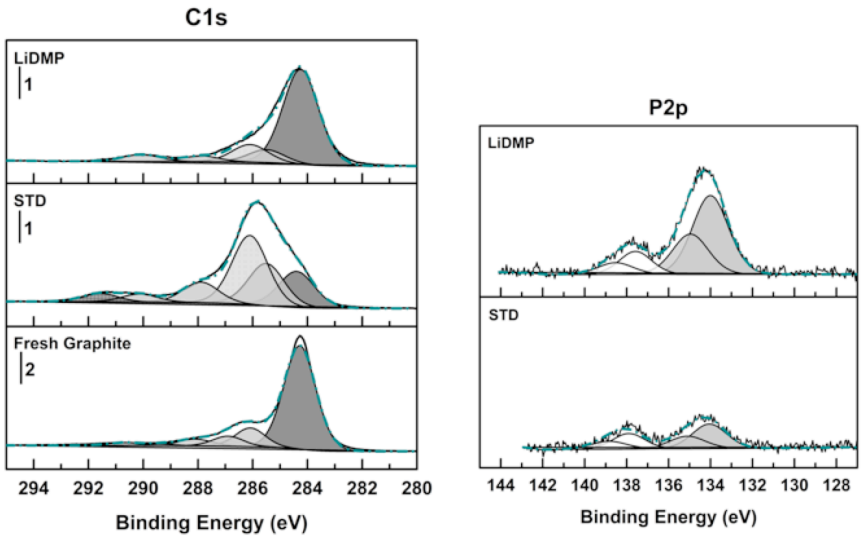

Figure 2.6: C1s core spectra of fresh graphite, graphite which has undergone formation at 25°C with the baseline electrolyte, and graphite which has undergone formation with the baseline electrolyte + LiDMP (left). P2p core spectra of graphite, which has undergone formation at 25°C

APPENDIX

Supplementary figures from the previous chapter are displayed on the following pages.

Figure a.1

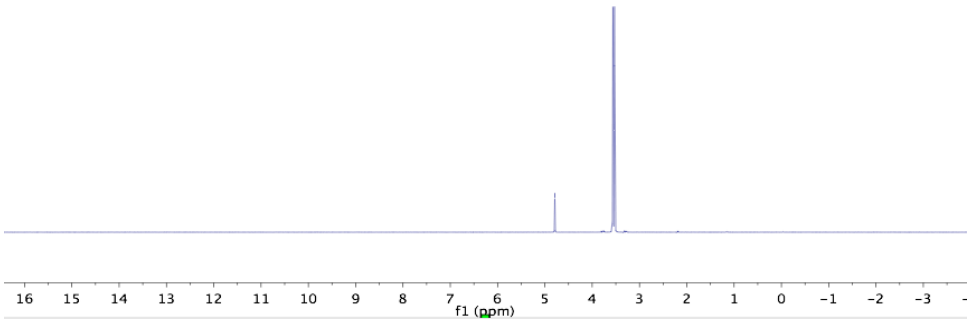

Figure a.1: ^{1}H NMR of LiDMP taken in D_2O

Figure a.2

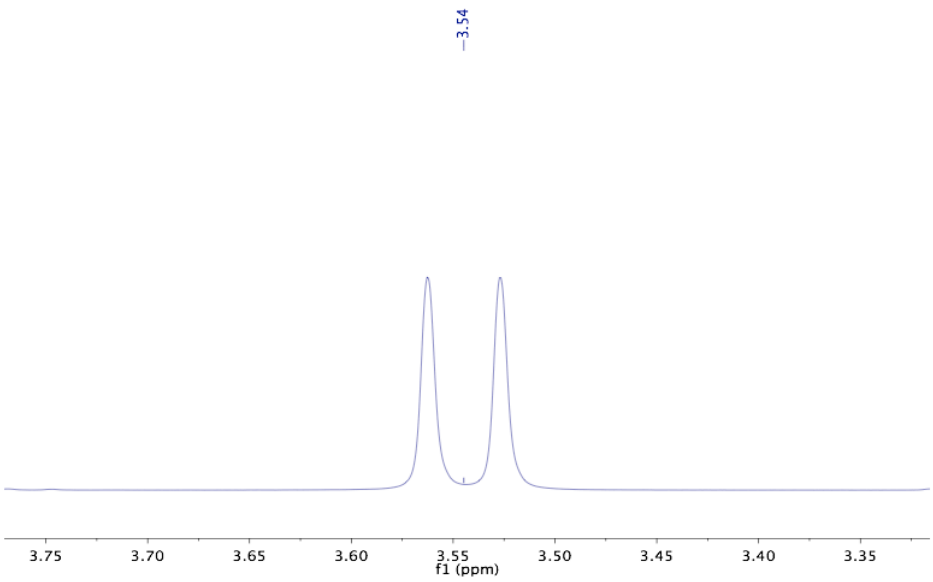

Figure a.2: ^{1}H NMR of LiDMP taken in D_2O

Figure a.3

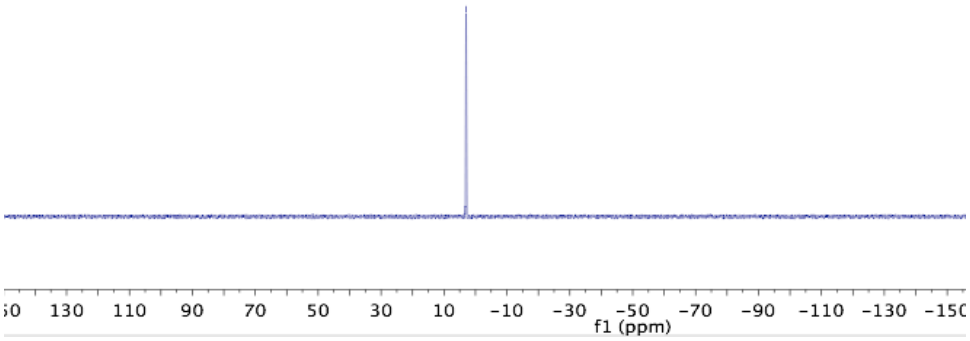

Figure a.3: ^{31}P NMR taken in D_2O

Figure a.4

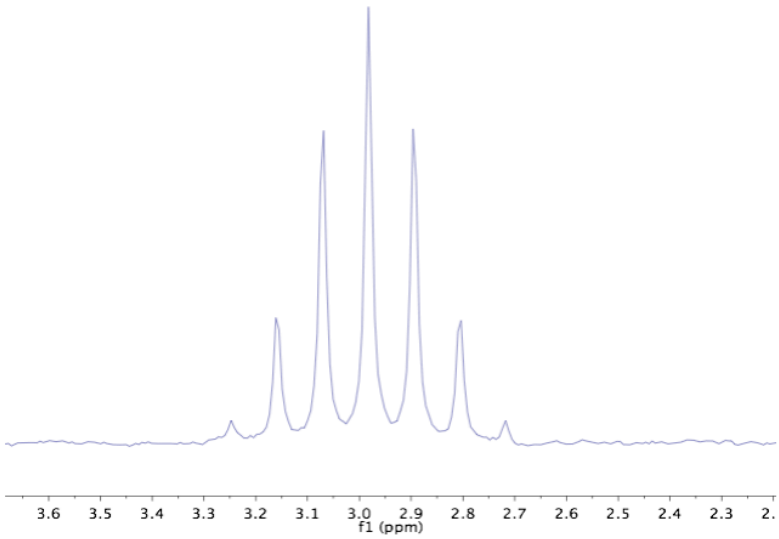

Figure a.4: ^{31}P NMR taken in D_2O

CHAPTER 3

LITHIUM BIS(2,2,2-TRIFLUOROETHYL)PHOSPHATE $Li[O_2P(OCH_2CF_3)_2]$: A NOVEL HIGH VOLTAGE ADDITIVE IN LNMO/GRAPHITE CELLS

by

M. S. Milien and B. L. Lucht

Manuscript in progress

PhD Candidate, Department of Chemistry, The University of Rhode Island, Kingston, RI 02882. Email: mmilien@chm.uri.edu

Professor, Department of Chemistry, The University of Rhode Island, Kingston, RI 02881. Email: blucht@chm.uri.edu

Abstract

The fluorinated phosphate lithium bis (2,2,2-trifluoroethyl) phosphate (LiBFEP) has been investigated as a film-forming additive employed to passivate the cathode and hinder continuous oxidation of the electrolyte. Incorporation of LiBFEP (0.1 and 0.5 wt %) into $LiPF_6$ in ethylene carbonate (EC)/ethyl methyl carbonate (EMC) (3:7 wt.) results in improved coulombic efficiency and capacity retention for LNMO/graphite cells. Ex-situ surface analysis of the electrodes suggests that incorporation of LiBFEP results in the formation of a cathode electrolyte interface (CEI) and modification of the solid electrolyte interface (SEI) on the anode. The formation of the CEI mitigates electrolyte oxidation and prevents the decomposition of $LiPF_6$, which in turn prevents HF-induced manganese dissolution from the cathode and destabilization of the SEI. The passivation of the cathode and stabilization of the SEI is responsible for the increased coulombic efficiency and capacity retention.

Introduction

Since their debut in 1991, commercial lithium ion batteries (LIB) have become the universal power source for consumer electronics.[1] Larger format LIB such as those needed to power electric vehicles (EV), an important niche market, have amassed considerable interest; however higher specific energy densities are required for larger format LIB.[1, 2] The practical way to increase energy density is to employ cathode materials with increased theoretical capacities and/or high discharge plateaus, and thus high energy (HE) or high voltage (HV) cathodes are required in order for LIB to meet the demands of the EV market.[3] While both HE and HV cathodes have been fabricated, current research efforts are focused on overcoming the caveats associated with these materials. The oxidative instability of carbonate-based electrolytes is a central limitation for cells with various cathode chemistries operated above 4.4V.[3-7] In addition to the instability of the electrolyte, cathodes such as nickel-rich layered oxides ($LiNi_xMn_yCo_zO_2$), lithium-rich layered oxides ($0.6Li_2MnO_3$-$0.4Li(Ni_{1/3}Co_{1/3}Mn_{1/3})O_2$), and HV spinel ($LiNi_{0.5}Mn_{1.5}O_4$) all suffer from structural instability when operated at high potentials.[5-8] While the layered oxides are capable of delivering higher practical energy densities, this work focuses on improving the performance of LNMO/Graphite cells.

The capacity fading observed in LNMO/Graphite cells is due to continuous oxidation of the electrolyte and transition metal dissolution.[3, 7] While the former results in electron loss and the formation of unstable species on the surface of the cathode, the latter results in destruction of the LNMO material (due to loss of manganese) and increased resistance of the SEI (due to deposition of manganese).[9,

12] Although research focused on altering the individual components (electrolyte solvents, electrolyte salts, and cathode material) prior to cell construction have been explored extensively, electrolyte additives have also been investigated to stabilize the existing electrolyte and/or passivate the cathode in-situ. The types of additives investigated in LNMO/Graphite cells are, but not limited to, borates, sultones, and anhydrides. Xu et. al. showed that borates lithium bis(oxolato)borate (LiBOB) and lithium tetramethyl borate (LTMB) displayed capacity retentions of 69% and 60%, respectively post 30 cycles at 55°C; in-situ gas analysis as well as ex-situ surface analysis revealed that LiBOB was sacrificially oxidized to generate a cathode passivation film (CEI) which decreased manganese dissolution while the improvement observed in the presence of LTMB was attributed to a borate-rich CEI (evidenced by XPS measurements) formed from the sacrificial oxidation of LTMB observed during the first cycle. [13-15] Lee et. al. showed that vinylene carbonate (VC) is a poor additive for the LNMO/Graphite system due to its poor anodic stability whereas 1,3-propane sultone (PS) and succinic anhydride (SA) both displayed capacity retentions greater than 50% post 200 cycles at 25°C compared to 36% capacity retention post 200 cycles with the STD; the improved performance was attributed to the formation of a stable, non-EC derived SEI. [16]

In this work the fluorinated phosphate, lithium bis(2,2,2-trifluoroethyl) phosphate $Li[O_2P(OCH_2CF_3)_2]$ (LiBFEP), will be evaluated as a film forming additive in the LNMO/graphite system.

Experimental

General

LiBFEP was synthesized in a two-step procedure as described by Schleep *et al*. [17].

Electrode preparation, cell assembly, and cycling of LNMO/Graphite full cells

Lithium ion coin cells containing an artificial graphite anode and $LiNi_{0.5}Mn_{1.5}O_4$ as the active cathode material were prepared with 1.2 M $LiPF_6$ in EC: EMC (3:7 by volume) with and without 0.1% (wt.) and 0.5% (wt.) added LiBFEP. The negative electrodes were composed of 95.7% (wt.) graphite, 3.8% (wt.) carboxymethyl cellulose (CMC) binder, and 0.5% (wt.) conductive carbon (Super P). The positive electrodes were composed of 92% (wt.) $LiNi_{0.5}Mn_{1.5}O_4$, 4% (wt.) polyvinylidene fluoride (PVDF) binder, and 4% (wt.) conductive carbon. The coin cells contained 90 μL electrolyte, 2 separators (a polyethylene film and a glass fiber), and were used for both electrochemical testing of the cells and *ex situ* analysis of the electrodes.

Coin cells were cycled with a constant current-constant voltage and a constant current discharge between 4.8 V and 3.3 V using a battery cycler (BT-2000 Arbin cycler, College Station, TX). The cells were cycled with the following formation procedure: first cycle at C/20, second and third cycles at C/10, and the fourth and fifth cycles at C/5. After the initial five formation cycles the cells were cycled at a C/5, rate for 195 cycles at room temperature.

Ex-situ Surface Analysis

The cells were disassembled in an argon glove box. The electrodes were rinsed with 500μl of dimethyl carbonate (DMC) twice to remove residual EC and $LiPF_6$ and

evacuated overnight prior to surface analysis. X-ray photoelectron spectroscopy (XPS) spectra were acquired with a K-alpha, Thermo system using Al Kα radiation (hυ = 1486.6 eV) under ultra high vacuum and a measured spot size of 400 μm. The binding energy was corrected based on the C 1s of C-C at 284.8 eV. The spectra obtained were analyzed by and fitted using Thermo Advantage software (version 5.926). A mixture of 30% Laurentzian and 70% Gaussian functions was used for the least-squares curves fitting procedure.

IR measurements were conducted on a Thermo Scientific Nicolet iS10 spectrometer with an attenuated total reflection (ATR) accessory. The electrodes were transferred from the argon glove box to the nitrogen-filled glove box in a sealed argon-filled vial. The spectra were acquired in a nitrogen glove box with a resolution of 4 cm^{-1} and a total of 512 scans.

Results and Discussion

Cycling of LNMO/Graphite full cells

Figure 3.1 displays the cycling performance and coulombic efficiency (CE) of LNMO/graphite cells cycled with the STD electrolyte, STD + 0.1 wt % LiBFEP, and STD + 0.5 wt % LiBFEP at 25 °C. Cells displayed first specific discharge capacities of 129.3 ± 0.3 mAh/g irrespective of the electrolyte formulation used. Cells cycled with the STD electrolyte displayed a first CE of 86%, the lowest capacity retention of the 3 formulations, and cell death after 196 cycles. Incorporation of 0.1 wt % of LiBFEP into the STD electrolyte doesn't alter the first CE (87%), however a small increase in capacity retention is observed, and the cells completed 200 cycles.

Increasing the concentration of LiBFEP to 0.5 wt % resulted in similar first CE (87%) to cells cycled with both the STD electrolyte and 0.1 wt % LiBFEP, however capacity fading decreased. Cells cycled with the STD displayed 73% capacity retention after 190 cycles, cells cycled with 0.1 wt % LiBFEP and 0.5 wt % LiBFEP displayed 76% and 79% capacity retention after 190 cycles, respectively. $LiPF_6$ decomposition generates HF, which is the root of Mn dissolution (detrimental to both the cathode and the anode), thus the improved capacity retention observed in the presence of LiBFEP is attributed to the stabilization of the SEI and the formation of a CEI.

Post -mortem analysis of LNMO and graphite electrodes with ATR-IR

In order to gain insight into LiBFEP's role in surface film formation, *ex situ* surface analysis of both electrodes were performed after formation cycling. Figure 3.2a displays ATR-IR spectra of graphite electrodes harvested from cells after formation cycling with the STD electrolyte, STD + 0.1 wt % LiBFEP, and STD + 0.5 wt % LiBFEP at 25 °C. The surface of graphite after formation cycling with the STD electrolyte contains absorptions consistent with the presence of Li_2CO_3 (1431 cm^{-1}) and $ROCO_2Li$ (1611 cm^{-1}).[18] While the surface of graphite post formation with LiBFEP also displays the Li_2CO_3 and $ROCO_2Li$ peaks, the intensities of these peaks are reduced significantly in the presence of LiBFEP. Additional peaks (1152 and 1206 cm^{-1}) are observed in the presence of LiBFEP, which are consistent with the presence of C-F, C-H, and P-O bonds [19] The intensity of these bands increase with increasing concentration of LiBFEP. Figure 3.2b displays ATR-IR spectra of LNMO electrodes harvested from cells after formation cycling with the STD electrolyte, STD

+ 0.1 wt % LiBFEP, and STD + 0.5 wt % LiBFEP at 25 °C. PVdF and residual EC are observed on the surface of LNMO irrespective of the electrolyte formulation used, however the 0.5 wt % LiBFEP spectrum has the lowest intensity of these bands. The PVdF binder bands are native to the LNMO cathode material, thus a decrease in the intensity of these bands suggests the presence of a surface film.

Post-mortem analysis of graphite and LNMO electrodes with XPS

In order to gain further understanding of LiBFEP's effect on the chemical composition of the graphite surface film, XPS surface analysis was carried out on graphite electrodes extracted from cells after formation cycling with the STD electrolyte, STD + 0.1 wt % LiBFEP, and STD + 0.5 wt % LiBFEP at 25 °C. The relative atomic concentrations of a fresh graphite electrode and graphite electrodes cycled with the 3 electrolyte formulations are displayed in Figure 3.3. In comparison to fresh graphite, the surface of graphite cycled with the STD electrolyte showed an increase in oxygen, a decrease in carbon, and additional fluorine, lithium, phosphorous, and Mn. This suggests the presence of a surface film consisting of electrolyte decomposition products (LiF, $Li_xPO_yF_z$, and Li_2CO_3) as well as Mn from the cathode. While the surface of graphite cycled with 0.1 wt % LiBFEP contained less carbon, oxygen, phosphorous, and manganese, increases in fluorine and lithium were detected. This suggests that the incorporation of 0.1 wt % LiBFEP into the STD electrolyte decreases manganese dissolution and results in a fluorine-rich SEI. The surface of graphite extracted from cells cycled with 0.5 wt % LiBFEP displayed the same trend in relative atomic concentrations as graphite cycled with 0.1 wt % LiBFEP,

however the increase in the concentration of LiBFEP resulted in a larger contribution from fluorine and lithium, The most notable difference is the complete absence of manganese with 0.5 wt % LiBFEP, demonstrating that LiBFEP is highly effective in preventing Mn dissolution.

Figure 3.4 displays XPS C1s, F1s, and Li1s core spectra of graphite electrodes harvested from cells post formation cycling (1: C/20; 2: C/10; and 2: C/5) with the STD, STD + 0.1 wt.% LiBFEP, and STD + 0.5 wt.% LiBFEP at 25°C. The surface of graphite cycled with the STD contains Li_2CO_3 (290.0 eV, C1s), $ROCO_2Li$ (286.5 and 288.8 eV, C1s), and LiF (685.0 eV, F1s), while the surface of graphite cycled with 0.1 wt.% LiBFEP contains $ROCO_2Li$ and LiF peaks. Instead of Li_2CO_3 and $ROCO_2Li$, the surface of graphite cycled with 0.5 wt.% LiBFEP displays CF_3 peaks (292.2 and 689.2eV, C1s and F1s, respectively) and an increase in LiF. This suggests a LiBFEP-derived surface film. The Mn3p (48.5 eV) peak observed in the Li1s spectrum of the STD is indicative of transition metal dissolution from the cathode.[20] A significant decrease in intensity of these peaks can be observed on the surface of graphite cycled with the 0.1 wt.% LiBFEP containing electrolyte, while these peaks are absent in the presence of 0.5 wt.% LiBFEP. This clearly demonstrates that LiBFEP suppresses transition metal dissolution. This can be accomplished in 3 ways: preventing HF formation, scavenging HF, or passivating the surface of the cathode.

In order to verify the presence of a CEI, XPS surface analysis was carried out on LNMO electrodes harvested from cells post formation cycling with the STD, STD + 0.1 wt.% LiBFEP, and STD + 0.5 wt.% LiBFEP at 25°C. The relative atomic concentrations of a fresh LNMO electrode and LNMO electrodes cycled with the three

electrolyte formulations are displayed in Figure 3.5. In comparison with fresh LNMO, a slight decrease in carbon and the addition of phosphorous was detected on the surface of LNMO electrodes cycled with the STD electrolyte. Less carbon and more fluorine was detected on the surface of LNMO electrodes cycled with 0.1 wt % LiBFEP than the surface of LNMO electrodes cycled with the STD electrolyte. The surface of LNMO electrodes cycled with 0.5 wt % LiBFEP contained less carbon and more fluorine and phosphorous than the surface of LNMO electrodes cycled with 0.1 wt % LiBFEP. The carbon detected on the surface of fresh LNMO electrodes is from the conductive carbon and the fluorine is from the PVdF binder. The decrease in carbon indicates the presence of a CEI on the surface of LNMO, while the increase in fluorine suggests the presence of fluorinated species (in addition to the PVdF binder). The combination of the decrease in carbon and increase in both fluorine and phosphorous detected with increased LiBFEP concentration suggests the presence of an LiBFEP-derived CEI, which increases in thickness as the concentration of the additive increases.

The C1s, O1s, and F1s core spectra of LNMO electrodes cycled with the three electrolyte formulations are displayed in Figure 3.6. While the surface of LNMO post formation with all 3 electrolyte formulations display LiF (685 eV, F1s) peaks, CF_3 peaks (292.2 and 689.2 eV, C1s and F1s, respectively) proportional to [LiBFEP] were detected on the surface of LNMO cycled with LiBFEP. This indicates the presence of a thin LiBFEP-derived surface film.

Conclusion

The implementation of LiBFEP as an additive in carbonate electrolytes improves the capacity retention of LNMO/graphite cells during long term cycling at room temperature. The increased coulombic efficiency of full cells and lack of manganese observed on the surface of graphite in the presence of LiBFEP all suggest the presence of a CEI. This was confirmed by XPS measurements of LNMO post formation cycling. Both XPS and IR measurements of graphite post formation cycling indicate that LiBFEP alters the SEI as well. The improved performance is attributed to a LiBFEP-derived CEI, which reduces electrolyte oxidation and prevents manganese dissolution from the cathode.

References

1. J. B. Goodenough, Rechargeable batteries: challenges old and new. *Journal of Solid State Electrochemistry* **16**, 2019-2029 (2012).
2. P. Meister *et al.*, Best Practice: Performance and Cost Evaluation of Lithium Ion Battery Active Materials with Special Emphasis on Energy Efficiency. *Chemistry of Materials* **28**, 7203-7217 (2016).
3. M. Hu, X. Pang, Z. Zhou, Recent progress in high-voltage lithium ion batteries. *Journal of Power Sources* **237**, 229-242 (2013).
4. N. Andreu *et al.*, XPS investigation of surface reactivity of electrode materials: effect of the transition metal. *ACS Appl Mater Interfaces* **7**, 6629-6636 (2015).
5. B. Xu, D. Qian, Z. Wang, Y. S. Meng, Recent progress in cathode materials research for advanced lithium ion batteries. *Materials Science and Engineering: R: Reports* **73**, 51-65 (2012).
6. R. Jung, M. Metzger, F. Maglia, C. Stinner, H. A. Gasteiger, Oxygen Release and Its Effect on the Cycling Stability of LiNixMnyCozO2(NMC) Cathode Materials for Li-Ion Batteries. *Journal of The Electrochemical Society* **164**, A1361-A1377 (2017).
7. R. A. Meyers, *Encyclopedia of Sustainability Science and Technology*. (2012).
8. M. Y. Son, J. K. Lee, Y. C. Kang, Fabrication and electrochemical performance of 0.6Li2MnO3-0.4Li(Ni1/3Co1/3Mn1/3)O2 microspheres by two-step spray-drying process. *Sci Rep* **4**, 5752 (2014).
9. T. Kozawa, T. Murakami, M. Naito, Insertion of lattice strains into ordered LiNi0.5Mn1.5O4 spinel by mechanical stress: A comparison of perfect versus

imperfect structures as a cathode for Li-ion batteries. *Journal of Power Sources* **320**, 120-126 (2016).

10. K. G. Gallagher *et al.*, Correlating hysteresis and voltage fade in lithium- and manganese-rich layered transition-metal oxide electrodes. *Electrochemistry Communications* **33**, 96-98 (2013).
11. N.-S. Choi, J.-G. Han, S.-Y. Ha, I. Park, C.-K. Back, Recent advances in the electrolytes for interfacial stability of high-voltage cathodes in lithium-ion batteries. *RSC Adv.* **5**, 2732-2748 (2015).
12. Z. Liu *et al.*, Conformal poly(ethyl α-cyanoacrylate) nano-coating for improving the interface stability of LiNi 0.5 Mn 1.5 O 4. *Electrochimica Acta* **236**, 221-227 (2017).
13. M. Xu *et al.*, Improving the Performance of Graphite/ LiNi0.5Mn1.5O4 Cells at High Voltage and Elevated Temperature with Added Lithium Bis(oxalato) Borate (LiBOB). *Journal of the Electrochemical Society* **160**, A2005-A2013 (2013).
14. M. Xu, N. Tsiouvaras, A. Garsuch, H. A. Gasteiger, B. L. Lucht, Generation of Cathode Passivation Films via Oxidation of Lithium Bis(oxalato) Borate on High Voltage Spinel (LiNi0.5Mn1.5O4). *The Journal of Physical Chemistry C* **118**, 7363-7368 (2014).
15. M. Xu *et al.*, Improved Performance of High Voltage Graphite/LiNi0.5Mn1.5O4 Batteries with Added Lithium Tetramethyl Borate. *ECS Electrochemistry Letters* **4**, A83-A86 (2015).

16. H. Lee *et al.*, SEI layer-forming additives for LiNi0.5Mn1.5O4/graphite 5V Li-ion batteries. *Electrochemistry Communications* **9**, 801-806 (2007).

17. Schleep *et al*., Synthesis, Characterization, and Electrochemical Investigation of Li[O2P(OCH2CF3)2] and Li[O2P{OC(H)(CF3)2}2] and Use of the Former for Coordination-Polymer-Based Gel Electrolytes. *ChemElectroChem* **3** (5), 774-782 (2016).

18. Aurbach *et al*., Recent studies on the correlation between surface chemistry, morphology, three-dimensional structures and performance of Li and Li-C intercalation anodes in several important electrolyte systems. *Journal of Power Sources* **68**, 91-98 (1997).

19. Pavia, D. L.; Lampman, G. M.; Kriz, G. S., Introduction to spectroscopy: A guide for students of organic chemistry, W.B. Saunders Co Philadelphia, (1979).

20. L. Bodenes *et al.*, Lithium-Ion Batteries Working at 85 C: Aging Phenomena and Electrode/Electrolyte Interfaces Studied by XPS. *Journal of the Electrochemical Society* **159**, A1739-A1746 (2012).

Figures

Figure 3.1

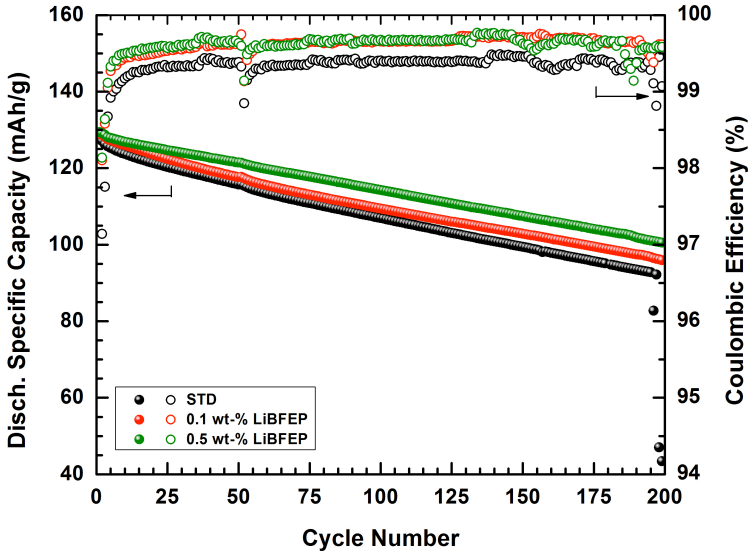

Figure 3.1: Cycling performance and coulombic efficiency of the STD electrolyte, STD + 0.1 wt % LiBFEP, and STD + 0.5 wt % LiBFEP in LNMO/graphite cells at 25 °C.

Figure 3.2

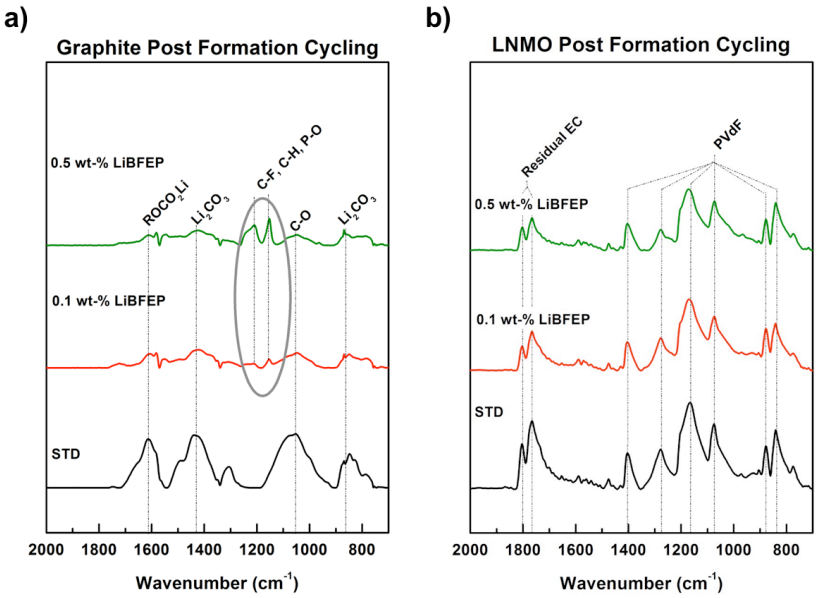

Figure 3.2: ATR-IR surface analysis of graphite (a) and LNMO (b) post formation cycling with the STD electrolyte, STD + 0.1 wt % LiBFEP, and STD + 0.5 wt % LiBFEP 25 °C.

Figure 3.3

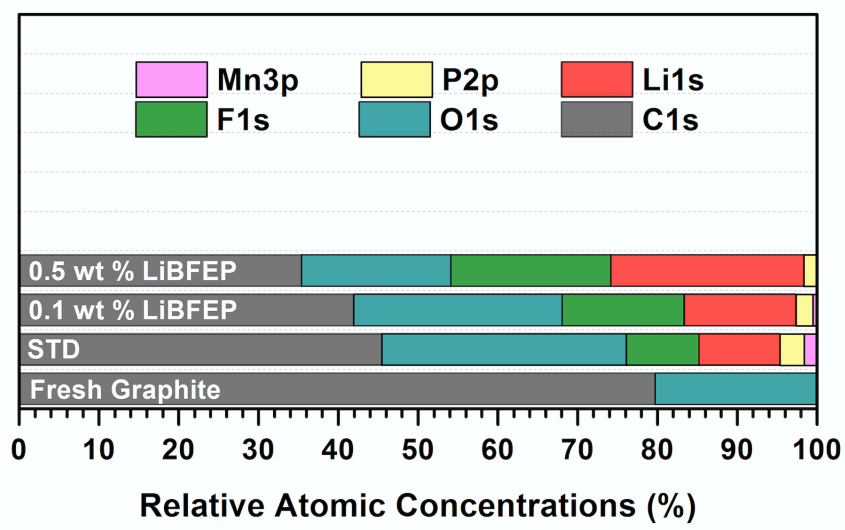

Figure 3.3: Relative atomic concentrations of a fresh graphite electrode, and graphite electrodes extracted after formation cycling with the STD electrolyte, STD + 0.1 wt % LiBFEP, and STD + 0.5 wt % LiBFEP at 25 °C.

Figure 3.4

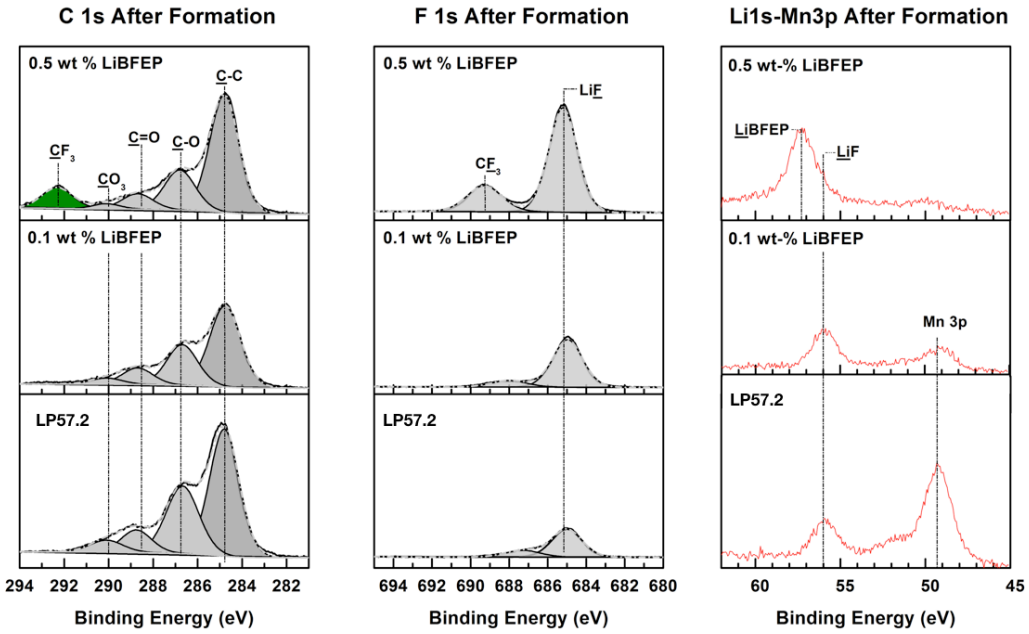

Figure. 3.4: XPS surface analysis of graphite post formation cycling with the STD electrolyte, STD + 0.1 wt % LiBFEP, and STD + 0.5 wt % LiBFEP at 25 °C.

Figure 3.5

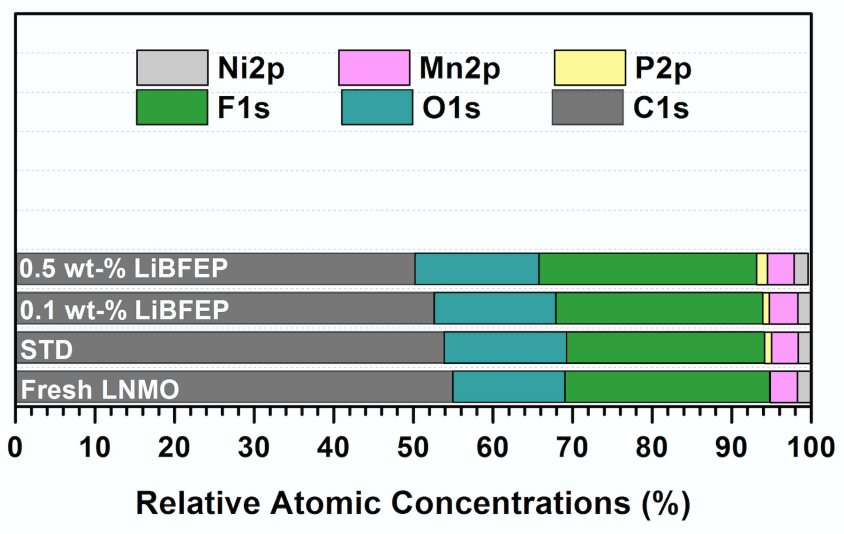

Figure. 3.5: Relative atomic concentrations of a fresh LNMO electrode, and LNMO electrodes extracted after formation cycling with the STD electrolyte, STD + 0.1 wt.-% LiBFEP, and STD + 0.5 wt.-% LiBFEP at 25 °C.

Figure 3.6

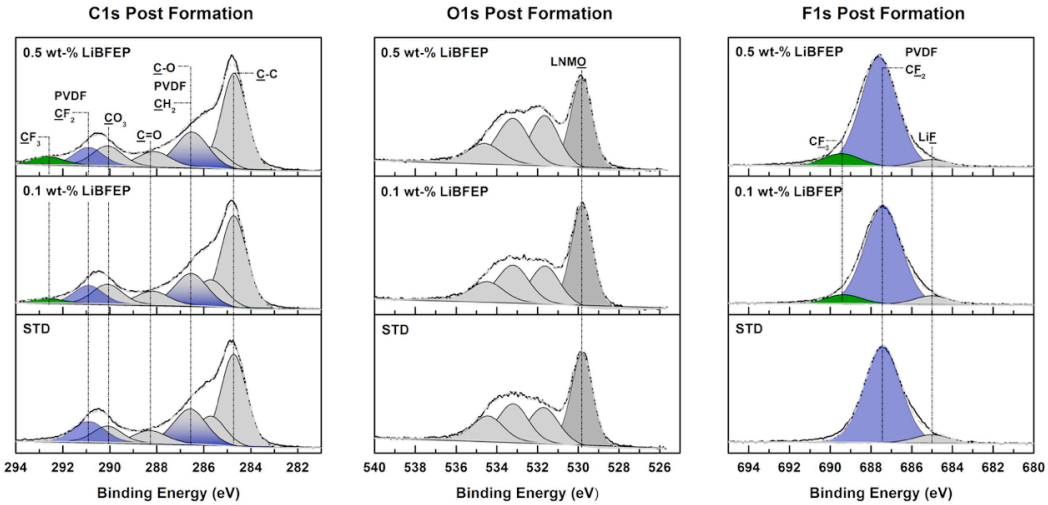

Figure. 3.6: XPS surface analysis of LNMO cathodes post formation cycling with the STD electrolyte, STD + 0.1 wt % LiBFEP, and STD + 0.5 wt % LiBFEP at 25 °C.

CHAPTER 4

THE EFFECTS OF ELECTROLYTE ADDITIVES ON Li4Ti5O12 AND HOW THEY IMPACT GASSING

by

Mickdy S. Milien[1]; Jenifer Hoffmann[2,3];Martin Payne[3]; Brett L. Lucht[4]

Manuscript in progress

---

[1] PhD Candidate, Department of Chemistry, The University of Rhode Island, Kingston, RI 02882. Email: mmilien@chm.uri.edu

[2] PhD Candidate, Department of Chemistry, The University of Rhode Island, Kingston, RI 02882.

[3] Battery R&D Gotion Inc, Ohio 44131, USA

[4] Professor, Department of Chemistry, The University of Rhode Island, Kingston, RI 02881. Email: blucht@chm.uri.edu

Abstract

Batteries consisting of $Li_4Ti_5O_{12}$ (LTO) anodes do not require the formation of a solid electrolyte interface to deliver robust high-rate performance at room temperature, however performance suffers at elevated temperatures due to gassing. Research has linked this gassing to the instability of the electrolyte on the surface of charged LTO at elevated temperatures. [1-3] If this is the case, a passivation layer, which prevents the electrolyte from coming into contact with the charged surface of LTO, should hinder gassing. Several classes of electrolyte additives have been investigated in $Li_4Ti_5O_{12}/LiMn_2O_4$ coin cells and pouch cells. ATR-IR and X-ray photoelectron spectroscopy has been used to gain an understanding of the surface films formed with different additives while in-situ gas measurements based on Archimedes' principle and gas chromatography have given insight into how the implementation of these additives affects gassing. The results from this study enable the selective design of surface films for LTO anodes, which reduces gassing at elevated temperatures without sacrificing performance.

Introduction

Graphite is the most ubiquitous anode material used in lithium ion batteries (LIB) when it comes to high energy density applications because of its low operating potential, low cost, and reasonable lifetime in standard conditions (moderate rates and temperature).[8] When it comes to high power density LIB such as those required for power tools, start-stop engines, or regenerative breaking, graphite is not suitable because of its limited rate capability and the safety concerns (lithium plating) associated with fast charging.[2, 9] Intrinsic characteristics of $Li_4Ti_5O_{12}$ (LTO) such as its high reduction potential (1.55 V vs. Li/Li^+) and lack of volume change during insertion/extraction (< 1%) coupled with the fact that its synthetic route has been optimized to render robust high rate capabilities and cycling stability makes LTO a very favorable anode material for high powered LIB.[8-10] Because LTO's high working potential narrows the voltage window of cells when paired with conventional cathode materials, LTO is currently most suitable for high-power applications. The principal challenge associated with the use of LTO anodes is the gassing of cells containing LTO both at elevated temperatures and when stored in the charged state. [9, 11-13]

Qin et. al reported that the predominant gas detected was H_2, the amount increased with temperature, and was only generated in cells containing LTO in the charged state.[14] Storage experiments of LTO in the charged state with and without $LiPF_6$ salt, also performed by Qin et. al., revealed that the amount of H_2 generated was reduced significantly in the absence of $LiPF_6$. Gassing measurements reported by Belharouck et. al. depicted an inverse relationship between H_2 generation and alkyl

gasses generated from electrolyte decomposition. [15] Since gaseous electrolyte decomposition products are likely to be accompanied by insoluble electrolyte decomposition products, which passivate the surface of LTO, this suggests that passivation of the electrode would decrease gassing. In addition to confirming more gassing at a higher state of charge, Liu et. al also demonstrated that cells stored in the presence of PC had less gassing than cells stored in the presence of EC. [11] This was attributed to the fact that the PC-based electrolyte formed thicker and denser SEI layers on LTO surfaces than EC-based electrolytes. While the presence of trace amounts of water in the electrolyte or the electrode was initially deemed the contributing factor to H_2 generation, the aforementioned results all suggest that the contact of the electrolyte with the charged surface of LTO is the problem. Various techniques such as coating, doping, poisoning, or passivating the surface of LTO to reduce gassing have been attempted. [16,14] This work focuses on using 2 classes of electrolyte additives (imides and borates) to passivate the surface of LTO and to employ both *in situ* and *ex situ* gassing measurements as well as *ex situ* surface analysis to gain an understanding of the effects of the additives.

Experimental

Materials

Battery grade ethylene carbonate (EC), propylene carbonate (PC), diethyl carbonate (DEC), lithium hexafluorophosphate ($LiPF_6$), LiTFSI, LiFSI, LiBOB, and LiDFOB were provided by a commercial supplier and used as received. TMSB was purchased from Sigma Aldrich and used as received.

Cell Preparation

Pouch cells – 920 mAh multilayer pouch cells were assembled by SKC using commercially available BTBM LMO as the cathode material and commercially available POSCO LTO as the anode material. The cells were dried at 55 °C for 12 hours under vacuum prior to filling. Once dried, cells were transferred to an argon glove box and filled with 9.1 g of electrolyte, baseline electrolyte is 1.0 M $LiPF_6$ in EC/PC/DEC (15:20:65), and vacuum sealed. All cells undergo 12 hours of rest at 25 °C after sealing to ensure complete wetting. Cycling data and gas measurements were obtained from pouch cells.

Coin cells – 2032- type coin cells with the same materials as the pouch cells were assembled in an argon glove box. While the coin cells cannot be degassed, adequate pressure applied by the spring's forces the gas into the headspace of the cell. The coin cells underwent the following formation procedure: constant current charge to 2.9 V at a 0.1C rate, held at a constant voltage for 2 hours at 2.9 V, allowed to rest for 10 minutes. Once the rest step was complete, cells were discharged to 2.1 V at a 0.1C rate, AC and DC impedance measurements were acquired, and the whole procedure was repeated. The coin cells have undergone the same high temperature storage and cycling protocol as the pouch cells. Surface analysis was carried out on electrodes extracted from coin cells.

Electrochemical Testing

Formation and Ageing – Pouch cells were clamped and cycled with a constant current (CC) charge at 0.1C with a 2.7 V cutoff using a MACCOR battery cycler. Once

charged, the cells were unclamped and placed in a 45 °C chamber for 12 hours of ageing. Cells were then degassed and vacuum-sealed in the argon glove box before undergoing a second formation step in which the cells were cycled with a constant current-constant voltage (CC-CV) charge and CC discharge between 2.8 and 1.7 V (vs. $Li_4Ti_5O_{12}/Li_7Ti_5O_{11}$) with the following procedure: 1 cycle at C/10, 1 cycle at C/5, and 1 cycle at 1C.

High Temperature Storage – After completing the formation and ageing procedure cells were clamped tightly and underwent the following storage procedure: charged with CC-CV to 2.8 V at 0.7C with a cutoff current of 0.02C, discharged with CC to 1.7 V at 1C, and charged with CC-CV to 2.8 V at 0.7 C with a cutoff current of 0.02C. The cells were then stored in the 100% state of charge (SOC) in a 60 °C chamber for 1 week. Upon completing the storage procedure cells experienced the following after storage procedure: discharged with CC to 1.7 V at 1C, charged with CC-CV to 2.8 V and finally discharged to 17 V at 1C.

Long Term Cycling – After completing the formation and ageing procedure, cells undergo rate testing between 2.8 and 1.7 V according to the following procedure: 2 cycles with C/2, D/2; 1 cycle with C/2, D/5; 1 cycle with C/2, D/2; 1 cycle with C/2, 1D; 1 cycle with C/2, 2D; and 3 cycles with C/2, D/2 (where C = charge rate and D = discharge rate). Once the rate testing is complete, cells undergo the before storage procedure described in the high temperature storage section, stored in the 100% SOC for 24 hours, and undergo the after storage procedure described in the high temperature storage section. Cells were transferred to a 45 °C chamber (tightly clamped) and cycled between 2.8 and 1.7 V at 1C with a C/10 cycle every 50 cycles.

All cells were prepared in duplicate to confirm reproducibility. Representative data are presented.

Gas Analysis

Gas Volume – Gas volume was measured before formation, before aging, after formation, after aging, before storage and/or cycling, and after storage and/or cycling according to the procedure first described by Aiken et al. [17] The pouch cells were hung from the bottom of a scale and tarred; after reaching a stable zero, the cells were submerged completely to a defined level in 25 °C deionized water. The recorded weight of the cell while submersed was then used along with the Archimedes' principle to calculate the amount of gas evolved over time

Gas Composition – To measure the composition of gasses, cells were brought into the argon dry box for extraction. A 0.5 mL Vici precision sampling analytical pressure-lock syringe was used to manually extract the gas sample from the cell under argon atmosphere. The sample was then manually injected into a Varian 450 gas chromatograph equipped with a 19808 Shin Carbon ST column, thermal conductivity detector (TCD), and argon was used as the carrier gas.

Ex-situ Surface Analysis

X ray Photoelectron Spectroscopy –The cells were disassembled in an argon glove box. The electrodes were rinsed with dimethyl carbonate (DMC) three times to remove residual EC and $LiPF_6$ and evacuated overnight prior to surface analysis. X-ray photoelectron spectroscopy (XPS) was acquired with a Thermo K-alpha system

using Al Kα radiation (hυ = 1486.6 eV) under ultra high vacuum and a measured spot size of 400 μm, and a 50.0 eV pass energy for the detector. Samples were transferred into the XPS chamber with a vacuum transfer vessel. The binding energy was corrected based on the C 1s of C-C at 284.3 eV. The spectra obtained were analyzed using Thermo Advantage software (version 5.926). A mixture of 30% Laurentzian and 70% Gaussian functions was used for the least-squares curves fitting procedure.

Results and Discussion

Although gasses formed during formation are typically removed from cells, gas analysis was carried out after formation and ageing with the various electrolyte formulations in order to compare the effects the various additives had on gassing. The results are depicted in Figure 4.2. The average gas volume for each formulation is displayed on the left and the gas composition for the corresponding electrolyte formulation is displayed on the right. With the exception of 2.0 wt % LiBOB the predominant gas observed is H_2. Pouch cells with 1.0 wt % LiTFSI, 1.0 wt % LiBOB, 2.0 wt % LiBOB, and 1.0 wt % TMSB all generated less gas than the baseline electrolyte, while cells cycled with 1.0 wt % LiFSI and 1.0 wt % LiDFOB generated more gas than the baseline electrolyte. With a 52.3 % reduction in gas, cells with 2.0 wt % LiBOB had the biggest impact on the volume of gas generated after formation and ageing. With the exception of 2.0 wt % LiBOB, the predominate gas detected after formation and ageing was H_2 (consistent with what has been reported in literature). [8, 12, 18] The amount of CO_2 detected increased in the presence of the oxalato borates, which are known to generate CO_2. [19]

XPS surface analysis was employed to characterize the surface of LTO electrodes after formation and ageing with the various electrolyte formulations. Figure 4.3 displays the relative atomic concentrations of LTO anodes after formation and ageing with all of the electrolyte formulations. Thin surface films (indicated by the Ti2p concentration) were detected on the surface of LTO in the presence of the baseline electrolyte, 1.0 wt % LiTFSI, and 1.0 wt % LiFSI. Although thicker boron containing surface films were detected on the surface of LTO in the presence of the borates, 1.0 wt % TMSB generated the thinnest film of the borates. In addition to thicker surface films on LTO, which underwent formation and ageing with the oxalato borates (1.0 wt % LiBOB, 2.0 wt % LiBOB, and 1.0 wt % LiDFOB), all surfaces have lower phosphorous and fluorine concentrations. This indicates less $LiPF_6$ decomposition in the presence of the borates.

Figure 4.4 provides C1s, O1s, and F1s core spectra of LTO electrodes extracted from cells after formation and ageing with the baseline electrolyte and the baseline + borate additives (1.0 wt % LiBOB, 2.0 wt % LiBOB, 1.0 wt % LiDFOB, and 1.0 wt % TMSB). The surface of LTO anodes cycled with the baseline electrolyte displays the thinnest film (based on the metal oxide peak (530.2 eV) in the O1s spectrum), which consists of electrolyte decomposition products Li_2CO_3 and LiF (290 eV, C1s and 685 eV F1s, respectively). The thinnest surface film for electrodes cycled with electrolytes containing borates was detected with 1.0 wt % TMSB, which consists of LiF and TMSB-derived species (based on the B1s concentration, see figure 4.3). The thickest surface films consisting of oxalates and LiF were observed in the presence of the oxalato borates. Due to the fact that LiDFOB contributes to the

generation of LiF, LTO electrodes cycled with 1.0 wt % LiDFOB contained more LiF than those cycled with either concentration of LiBOB.

Since gassing of cells containing LTO is reported to be a result of the instability of the electrolyte on the charged surface of LTO at elevated temperatures, cells which have undergone the formation and ageing procedure with the various additive-containing electrolyte formulations were degassed, resealed and stored in the 100% SOC for 1 week at 60 °C. The gas analysis results are depicted in Figure 4.5. The average gas volume is displayed on the left, while the gas composition is displayed on the right. As far as the volume of gas generated, pouch cells with 1.0 wt % TMSB were the only electrolyte formulations that reduced gassing after storage. Incorporating 1.0 wt % of TMSB into the baseline electrolyte decreased gassing by 5.22% after 1 week of storage at 60 °C. As far as gas composition, the predominant gas detected irrespective of the electrolyte formulation used was H_2. Cells that were stored for 1 week with the oxalato borates generated more CO_2 than the others, while the hydrocarbon gasses (CH_4, C_2H_4, and C_2H_6) were only detected in the absence of the oxalato borates. This suggests that while incorporating the oxalato borates into the baseline electrolyte contributes to CO_2 generation, it also hinders parasitic reactions with the electrolyte solvents.

In order to gain insight into the composition of the surface film on LTO anodes after 1 week of storage at 60 °C XPS surface analysis was performed on LTO electrodes extracted from cells that have been stored with the various electrolyte formulations. Based on the concentration of titanium, the thinnest surface film was detected on the LTO anode stored with 1.0 wt % LiFSI, the thickest surface films were

detected on LTO anodes stored with the oxalato borates, and LTO anodes stored with 1.0 wt % TMSB had the thinnest surface film of all cells stored with the borates. Manganese was only detected on the surface of LTO anodes stored in the absence of the borate additives. This suggests that the borate additives prevented manganese dissolution from the LMO cathodes during 1 week of storage at 60 °C.

C1s, O1s, and F1s core spectra of LTO anodes extracted from cells after 1 week of storage at 60 °C are displayed in Figure 4.7. A thin surface film (based on the intensity of the metal oxide peak; 530.2 eV, O1s) consisting of LiF (685 eV, F1s) was detected on the LTO anode stored with the baseline electrolyte. LTO anodes stored with 1.0 wt % LiFSI had the thinnest surface film, which consisted of LiF. The thickest surface film consisting of oxalates and LiF was detected on the surface of LTO anodes stored with 1.0 wt % LiBOB. LTO anodes stored with 1.0 wt % LiDFOB displayed a thick surface film consisting of oxalates and LiF. Cells stored with 1.0 wt % TMSB had the thinnest surface film of the borates, which consisted of TMSB-derived species (B1s).

While the focus of this work was to determine if and how the use of electrolyte additives to passivate LTO anodes affects gassing, the impact of the additives on cycling stability should not be overlooked. For this reason LTO/LMO pouch cells were assembled with the various electrolyte formulations and cycled at 45 °C for 600 cycles. The cells underwent 1 cycle at a 0.1C rate (formation), degassed, and re-sealed. The remaining cycles were carried out at a 1C rate, and the resulting cycling performance is shown in Figure 8a. Although cells cycled with 1.0 wt % LiFSI displayed the best performance of all the additives, it was on par with the performance

observed with the baseline electrolyte. Cells cycled with 1.0 wt % LiTFSI, 1.0 wt % LiBOB, and 1.0 wt % LiDFOB had less capacity than cells cycled with the baseline electrolyte prior to 300 cycles, however cells cycled with 1.0 wt % LiBOB and 1.0 wt % LiTFSI had similar capacities to cells cycled with the baseline electrolyte after 600 cycles. Increasing the concentration of LiBOB by 1.0 wt % resulted in a drop in capacity and cells cycled with 1.0 wt % TMSB displayed the worst capacity of all the additives. Capacity retention is plotted in Figure 8b. While cells cycled with the imides had higher initial capacities (see Figure 4.8a), cells cycled with the oxalato borates were superior to those cycled with the imides as far as capacity retention is concerned. Cells cycled with the formulations which formed the thinnest surface films (1.0 wt % LiFSI, 1.0 wt % LiTFSI, and 1.0 wt % TMSB) displayed the most capacity fading, while those cycled with the oxalato borates displayed the least fading. This clearly demonstrates that passivating the surface of LTO is actually beneficial to cycling stability. It should be noted that the spikes observed during cycling at cycle 300 are a result of the cells being stopped for gassing measurements and resumed afterwards.

The volume of gas evolved during cycling was measured after 300 cycles and again after 600 cycles. The results are displayed in Figure 4.9. While cells cycled with 1.0 wt % LiBOB and 1.0 wt % TMSB both generated less gas than cells cycled with the baseline electrolyte after 300 cycles, cells cycled with 1.0 wt % TMSB were the only ones that displayed reduced gassing after 600 cycles.

Conclusion

While better cycling performance was observed in the presence of the imides, the thinnest surface films and consequently more gassing was observed. The oxalato borates formed the thickest surface films, and less H_2 was detected, however the oxalato borates are known for generating CO_2, thus gassing is not reduced overall. Less gassing was detected in the presence of TMSB in all cases, however TMSB displays the worst capacity retention of all the additives. The presence of the hydrocarbon gasses, LiF, and $Li_xPO_yF_z$ combined with the pronounced fading observed with LiTFSI, LiFSI, and TMSB suggests that these additives react with the electrolyte. Nonetheless, less gassing was observed in the presence of TMSB. Optimization of additive concentration and further experiments are underway.

References

1. Meyers, R. A., *Encyclopedia of Sustainability Science and Technology*. 2012.
2. Goodenough, J. B., Rechargeable batteries: challenges old and new. *Journal of Solid State Electrochemistry* **2012,** *16* (6), 2019-2029.
3. Hu, M.; Pang, X.; Zhou, Z., Recent progress in high-voltage lithium ion batteries. *Journal of Power Sources* **2013,** *237*, 229-242.
4. Schleep, M.; Reininger, S.; Eiden, P.; Klose, P.; Schulz, C.; Scherer, H.; Laule, S.; Bodendorfer, S.; Schmidt, M.; Garsuch, A.; Krossing, I., Synthesis, Characterization, and Electrochemical Investigation of Li[O2P(OCH2CF3)2] and Li[O2P{OC(H)(CF3)2}2] and Use of the Former for Coordination-Polymer-Based Gel Electrolytes. *ChemElectroChem* **2016,** *3* (5), 774-782.
5. Metzger, M.; Sicklinger, J.; Haering, D.; Kavakli, C.; Stinner, C.; Marino, C.; Gasteiger, H. A., Carbon Coating Stability on High-Voltage Cathode Materials in H2O-Free and H2O-Containing Electrolyte. *Journal of the Electrochemical Society* **2015,** *162* (7), A1227-A1235.
6. Bodenes, L.; Dedryvere, R.; Martinez, H.; Fischer, F.; Tessier, C.; Peres, J. P., Lithium-Ion Batteries Working at 85 C: Aging Phenomena and Electrode/Electrolyte Interfaces Studied by XPS. *Journal of the Electrochemical Society* **2012,** *159* (10), A1739-A1746.
7. Banerjee, A.; Shilina, Y.; Ziv, B.; Ziegelbauer, J. M.; Luski, S.; Aurbach, D.; Halalay, I. C., Review—Multifunctional Materials for Enhanced Li-Ion Batteries Durability: A Brief Review of Practical Options. *Journal of The Electrochemical Society* **2017,** *164* (1), A6315-A6323.

8. Han, C.; He, Y.-B.; Liu, M.; Li, B.; Yang, Q.-H.; Wong, C.-P.; Kang, F., A review of gassing behavior in Li4Ti5O12-based lithium ion batteries. *J. Mater. Chem. A* **2017,** *5* (14), 6368-6381.

9. Xu, G.; Han, P.; Dong, S.; Liu, H.; Cui, G.; Chen, L., Li 4 Ti 5 O 12 -based energy conversion and storage systems: Status and prospects. *Coordination Chemistry Reviews* **2017,** *343*, 139-184.

10. Chen, S.; Xin, Y.; Zhou, Y.; Ma, Y.; Zhou, H.; Qi, L., Self-supported Li4Ti5O12 nanosheet arrays for lithium ion batteries with excellent rate capability and ultralong cycle life. *Energy & Environmental Science* **2014,** *7* (6).

11. Liu, J.; Bian, P.; Li, J.; Ji, W.; Hao, H.; Yu, A., Gassing behavior of lithium titanate based lithium ion batteries with different types of electrolytes. *Journal of Power Sources* **2015,** *286*, 380-387.

12. Lv, W.; Gu, J.; Niu, Y.; Wen, K.; He, W., Review—Gassing Mechanism and Suppressing Solutions in Li4Ti5O2
-Based Lithium-Ion Batteries. *Journal of The Electrochemical Society* **2017,** *164* (9), A2213-A2224.

13. He, M.; Castel, E.; Laumann, A.; Nuspl, G.; Novak, P.; Berg, E. J., In Situ Gas Analysis of Li4Ti5O12 Based Electrodes at Elevated Temperatures. *Journal of the Electrochemical Society* **2015,** *162* (6), A870-A876.

14. <Functionalized Surface Modification Agents to Sup- press Gassing Issue of Li4 Ti5 O12 -Based Lithium-Ion Chemistry.pdf>.

15. Belharouak, I.; Koenig, G. M.; Tan, T.; Yumoto, H.; Ota, N.; Amine, K., Performance Degradation and Gassing of Li4Ti5O12/LiMn2O4 Lithium-Ion Cells. *Journal of the Electrochemical Society* **2012,** *159* (8), A1165-A1170.

16. Li, X.; Zhao, X.; Huang, P.-x.; Wang, M.-s.; Huang, Y.; Zhou, Y.; Lin, Y.-h.; Qu, M.-z.; Yu, Z.-l., Enhanced electrochemical performance of SrF2-modified Li4Ti5O12 composite anode materials for lithium-ion batteries. *Journal of Alloys and Compounds* **2017,** *693*, 61-69.

17. Aiken, C.P.; Xia, J.; Wang, D.Y.; Stevens, D.A.; Trussler, S.; Dahn, J.R., An apparatus for the study of in situ gas evolution in Li-ion pouch cells, *Journal of Electrochemical Society* **2014,** 161, A1548-A1554.

18. He, Y. B.; Li, B.; Liu, M.; Zhang, C.; Lv, W.; Yang, C.; Li, J.; Du, H.; Zhang, B.; Yang, Q. H.; Kim, J. K.; Kang, F., Gassing in Li(4)Ti(5)O(12)-based batteries and its remedy. *Sci Rep* **2012,** *2*, 913.

19. Xu, M.; Tsiouvaras, N.; Garsuch, A.; Gasteiger, H. A.; Lucht, B. L., Generation of Cathode Passivation Films via Oxidation of Lithium Bis(oxalato) Borate on High Voltage Spinel (LiNi0.5Mn1.5O4). *The Journal of Physical Chemistry C* **2014,** *118* (14), 7363-7368.

Figures

Figure 4.1

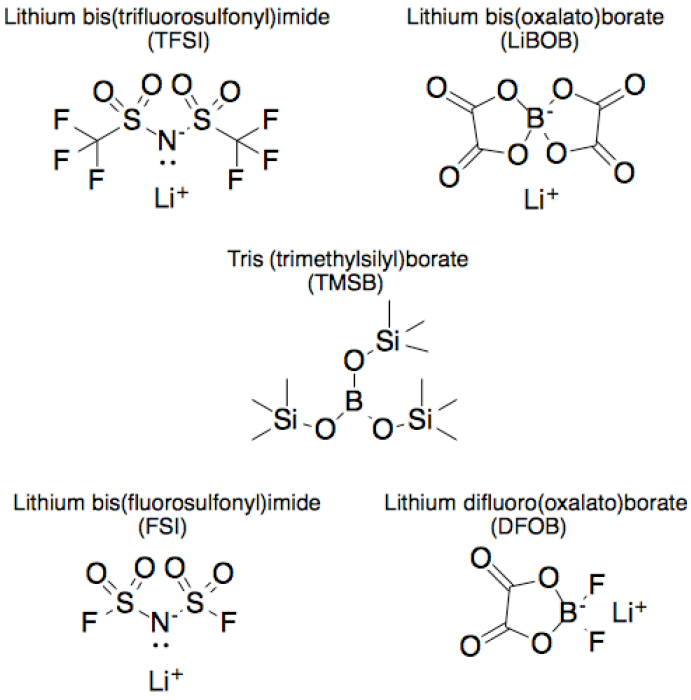

Figure 4.1: Chemical Structures of LiTFSI, LiFSI, LiBOB, TMSB, and LiDFOB.

Figure 4.2

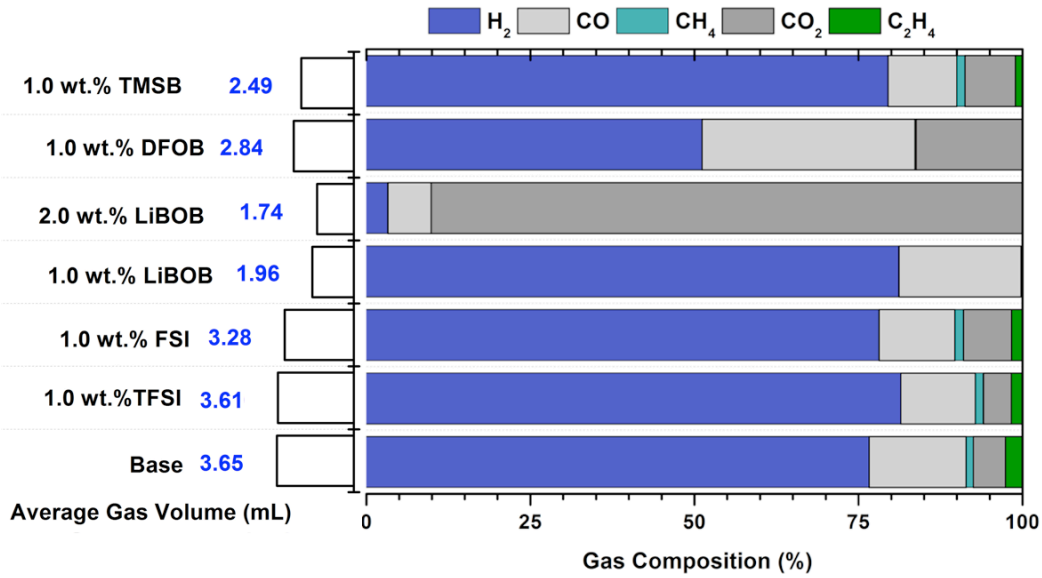

Figure 4.2: Average volume of gas (left) and composition of gas generated after formation and ageing with the Base electrolyte, baseline + 1.0 wt % LiTFSI, baseline + 1.0 wt % LiFSI, baseline + 1.0 wt % LiBOB, baseline + 2.0 wt % LiBOB, baseline + 1.0 wt % LiDFOB, and baseline + 1.0 wt % TMSB.

Figure 4.3

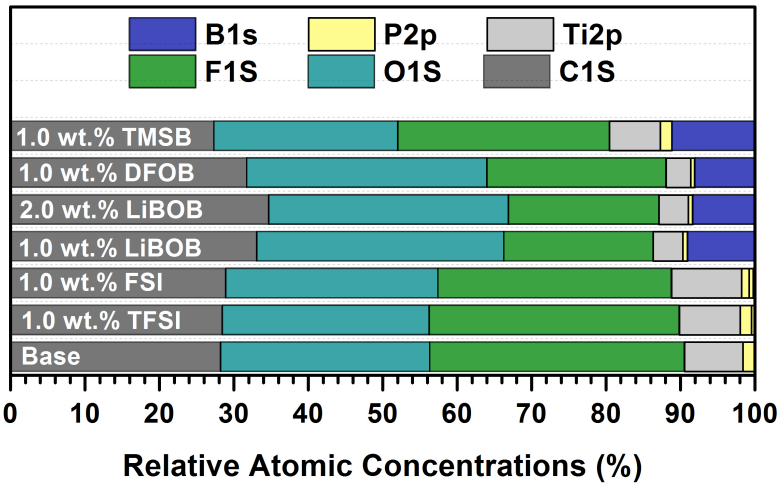

Figure 4.3: Relative atomic concentrations of elements detected on the surface of LTO electrodes after formation and ageing with the baseline electrolyte, baseline + 1.0 wt % LiTFSI, baseline + 1.0 wt % LiFSI, baseline + 1.0 wt % LiBOB, baseline + 2.0 wt % LiBOB, baseline + 1.0 wt % LiDFOB, and baseline + 1.0 wt % TMSB.

Figure 4.4

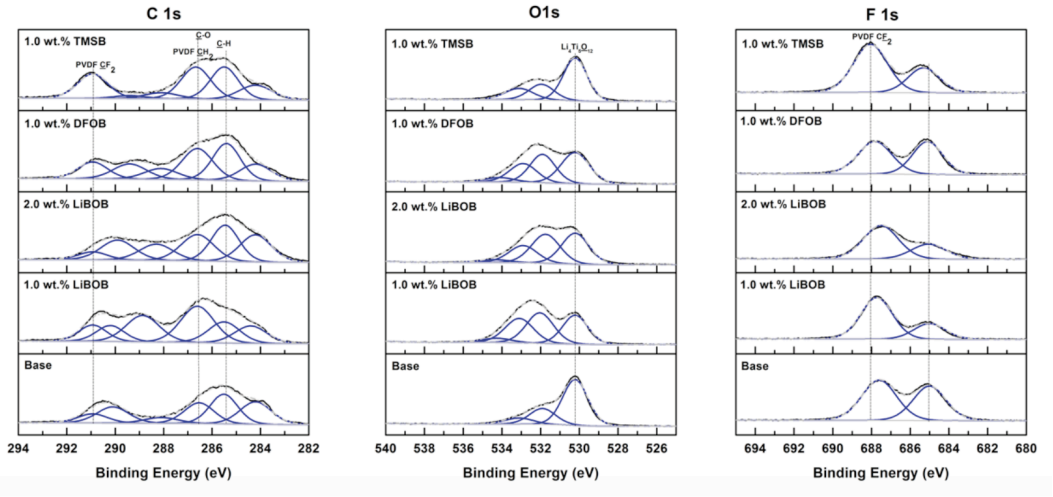

Figure4. 4: C 1s, O 1s, and F 1s core spectra of LTO electrodes after formation and ageing with the Base electrolyte, baseline + 1.0 wt % LiBOB, baseline + 2.0 wt % LiBOB, baseline + 1.0 wt % LiDFOB, and baseline + 1.0 wt % TMSB.

Figure 4.5

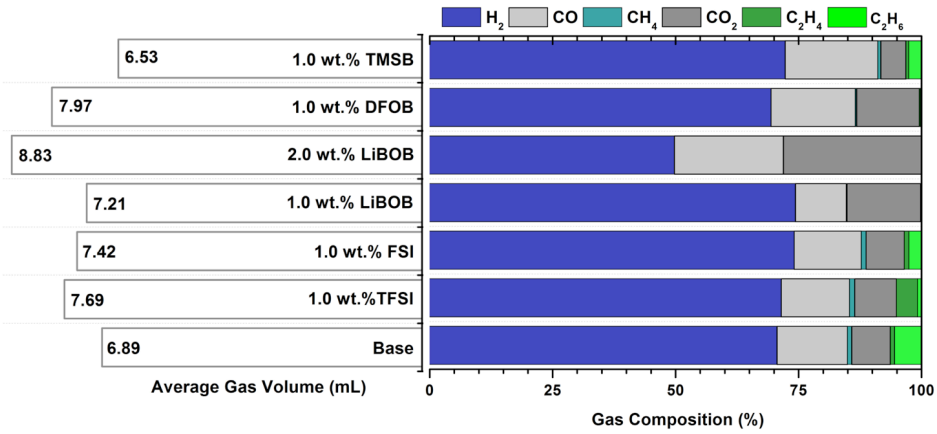

Figure 4.5: Average volume of gas (left) and composition of gas generated after formation, ageing, and 1 week of storage at 60 °C with the baseline electrolyte, baseline + 1.0 wt % LiTFSI, baseline + 1.0 wt % LiFSI, baseline + 1.0 wt % LiBOB, baseline + 2.0 wt % LiBOB, baseline + 1.0 wt % LiDFOB, and baseline + 1.0 wt % TMSB

Figure 4.6

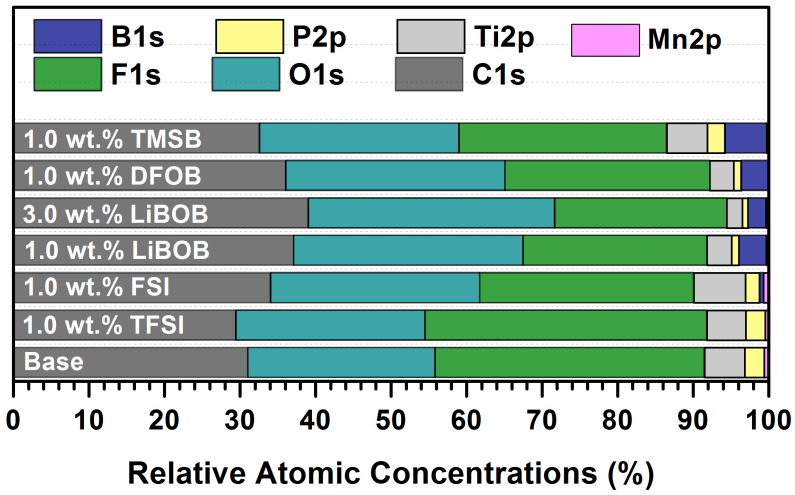

Figure 4.6: Relative atomic concentrations of elements detected on the surface of LTO electrodes after formation, ageing, and 1 week of storage at 60 °C with the baseline electrolyte, baseline + 1.0 wt % LiTFSI, baseline + 1.0 wt % LiFSI, baseline + 1.0 wt % LiBOB, baseline + 3.0 wt % LiBOB, baseline + 1.0 wt % LiDFOB, and baseline + 1.0 wt % TMSB.

Figure 4.7

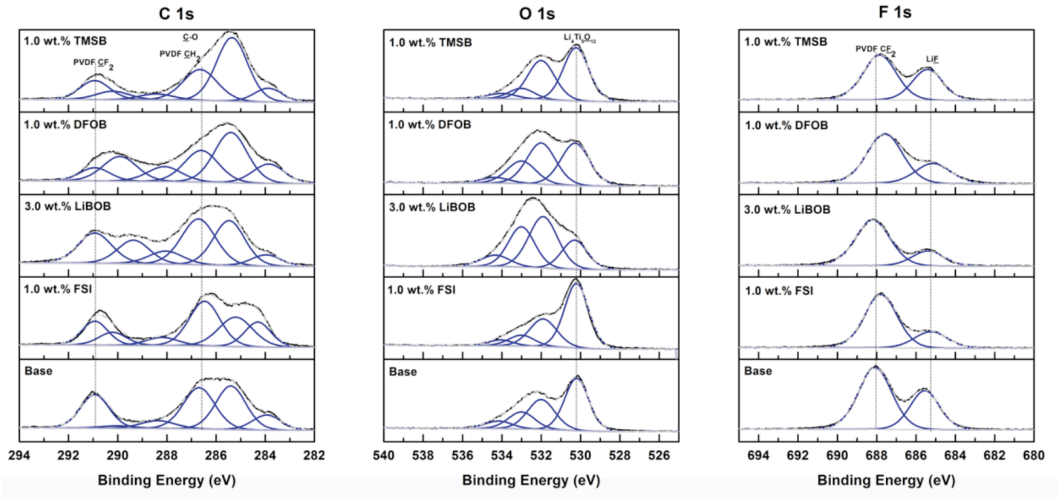

Figure 4.7: C 1s, O 1s, and F 1s core spectra of LTO electrodes after formation, ageing, and 1 week of storage at 60 °C with the baseline electrolyte, baseline + 1.0 wt % LiFSI, baseline + 3.0 wt % LiBOB, baseline + 1.0 wt % LiDFOB, and baseline + 1.0 wt % TMSB.

Figure 4.8

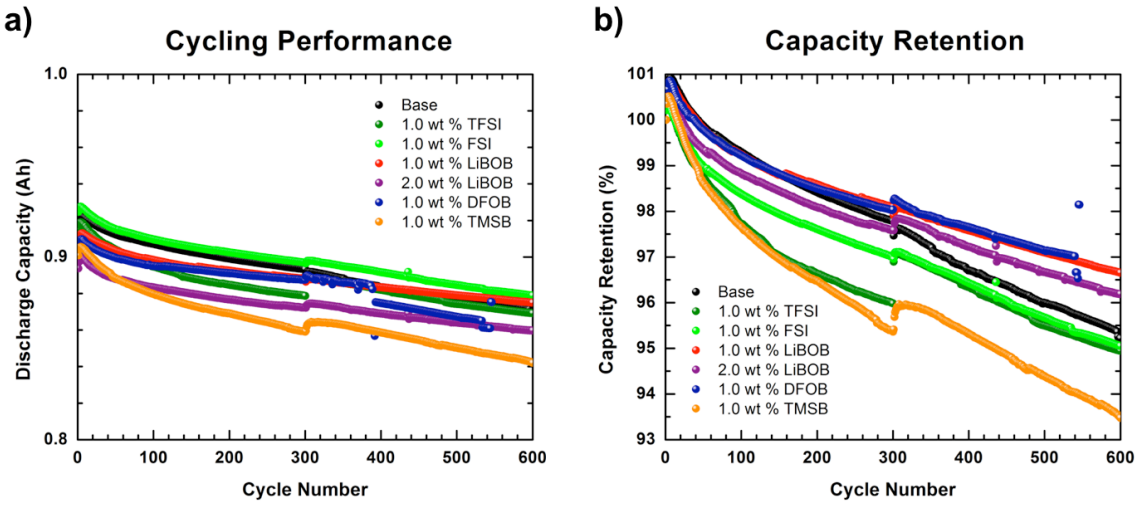

Figure 4.8: Capacity retention (a) relative capacity retention (b) of long term cycling at 45 °C with the baseline electrolyte, baseline + 1.0 wt % LiTFSI, baseline + 1.0 wt % LiFSI, baseline + 1.0 wt % LiBOB, baseline + 2.0 wt % LiBOB, baseline + 1.0 wt % LiDFOB, and baseline + 1.0 wt % TMSB.

Figure 4.9

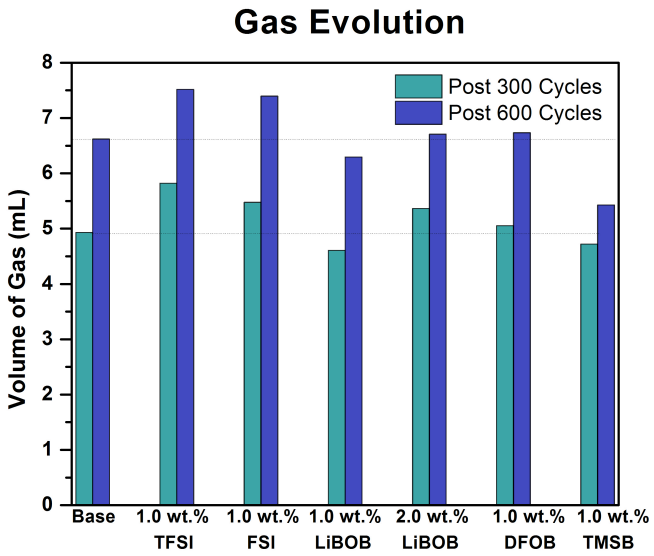

Figure 4.9: Volume of gas generated after 300 and 600 cycles at 45 °C with the baseline electrolyte, baseline + 1.0 wt % LiTFSI, baseline + 1.0 wt % LiFSI, baseline + 1.0 wt % LiBOB, baseline + 2.0 wt % LiBOB, baseline + 1.0 wt % LiDFOB, and baseline + 1.0 wt % TMSB.